FACULDADE DE ENGENHARIA DA UNIVERSIDADE DO PORTO

Inflatable Reflector Antenna

Mafalda Ho de Almeida Santos

Mestrado Integrado em Engenharia Electrotécnica e de Computadores

Orientador: Sérgio Reis Cunha (PhD)

22nd July, 2021

Resumo

SARIA (Radar de Abertura Sintética usando uma Antena Insuflável) é uma experiência selecionada para voar num balão estratosférico, no âmbito do programa REXUS/BEXUS ciclo 13, e utilizará uma antena insuflável, operando a 5.8 GHz, para criar imagens de radar de abertura sintética (SAR). Vários problemas, como a seleção de material, impediram a SARIA de desenvolver uma antena insuflável operacional. O objetivo desta dissertação é projetar e implementar uma antena parabólica refletora insuflável, a 5.8 GHz, com um diâmetro de 1 m, bem como controlar a pressão da antena insuflável usando um sistema de inflação ativo.

Este trabalho usa métodos de elementos finitos (FEM) para auxiliar nas fases iniciais de desenvolvimento de uma antena insuflável. Para simular o formato da antena insuflável, com diversos valores de pressão diferencial, foi escolhido o software de análise de elementos finitos (FEA) *Abaqus/FEA* . Um script *Matlab* foi utilizado para determinar o padrão de radiação de uma antena insuflável. Como resultado, é possível estimar o intervalo de pressão diferencial ideal e caracterizar as propriedades radio-frequência (RF) de uma antena insuflável antes do seu fabrico. Usando estas ferramentas, propõe-se uma nova modificação de design para a antena insuflável da SARIA. Uma antena insuflável é fabricada manualmente usando Mylar® para a parte refletora e plástico transparente para a cobertura. A pressão desta antena é controlada por um sistema de inflação ativo, responsável por manter a pressão diferencial da antena insuflável dentro de um intervalo ótimo.

Foi obtida uma antena insuflável com ganho de 23.77 dBi a 5.8 GHz. A sua caracterização revelou uma perda de ganho de 5.6 dBi, em relação ao ganho simulado, devido a dificuldades de implementação, nomeadamente do processo de fabrico, que são explicadas na tese. Este trabalho contribui, assim, para o *know-how* de desenvolvimento de antenas insufláveis para aplicações de baixa pressão e em ambiente orbital.

Abstract

SARIA (Synthetic-Aperture Radar using an Inflatable Antenna) is an experiment selected to fly in a stratospheric balloon, in the scope of the REXUS/BEXUS programme cycle 13, and will use an inflatable antenna, operating at 5.8 GHz, to create Synthetic-Aperture Radar (SAR) images. Several problems, such as material selection, have prevented SARIA from developing an operational inflatable antenna. The objective of this dissertation is to design and implement an inflatable parabolic reflector antenna, at 5.8 GHz, with a diameter of 1 m as well as to control the inflatable antenna pressure using an active inflation system.

This work uses Finite Element Method (FEM) to assist on the initial developing phases of an inflatable antenna. To simulate the inflatable antenna shape, at several differential pressure values, the Finite Element Analysis (FEA) software *Abaqus/FEA* was chosen. A *Matlab* script was used to compute the radiation pattern of an inflatable antenna. As a result, it is possible to estimate the optimal differential pressure interval and characterize the Radio Frequency (RF) properties of an inflatable antenna prior to manufacturing. Using these tools, a new design modification for SARIA inflatable antenna is proposed. An inflatable antenna is manufactured by hand using Mylar® for the reflective part and transparent plastic for the canopy. The pressure of this antenna is controlled by an active inflation system which is responsible for keeping the inflatable antenna differential pressure inside an optimal interval.

An inflatable antenna with a gain of 23.77 dBi at 5.8 GHz was obtained. Its characterization has revealed a gain loss of 5.6 dBi, in respect to the simulated gain, due to implementation difficulties, namely the manufacturing process, which are explained in the thesis. This work contributes to the expertise of developing inflatable antennas for low pressure applications and in orbital environment applications.

Agradecimentos

Ao meu orientador, Professor Sérgio Reis Cunha, pela sua dedicação e conhecimento transmitido ao longo da realização deste trabalho. Ao Nuno Barros pela sua prontidão e conhecimentos partilhados. Aos meu pais e irmão pela sua paciência e apoio em garantir as condições propícias à realização deste trabalho. Aos meus amigos e equipa do SARIA que me acompanharam na realização desta dissertação.

Mafalda Santos

"When you're curious, you find lots of interesting things to do."

Walt Disney

Contents

List of Figures

List of Tables

Abbreviations and Symbols

ADC Analog-to-Digital Converter

AUT Antenna Under Test

BEXUS Balloon EXperiments for University Students

COTS Commercially Available Off-The-Shelf

CRC Cyclic Redundacy Check

FAIM Finite Element Analysis of Inflatable Membranes

FEA Finite Element Analysis

FEM Finite Element Method

FET Field Effect Transistor

GPS Global Positioning System

IAE Inflatable Antenna Experiment

IMU Inertial Measurement Unit

IPRA Inflatable Parabolic Reflector Antenna

MCU Microcontroller Unit

MSL Mean Sea Level

NASA National Aeronautics and Space Administration

PCB Printed Circuit Board

PET Polyethylene Terephthalate

RF Radio Frequency

RMS Root Mean Square

SAR Synthetic-Aperture Radar

SARIA Synthetic-Aperture Radar using an Inflatable Antenna

SDR Software Defined Radio

SI International System of Units

VNA Vector Network Analyzer

Chapter 1

Introduction

This chapter is used to provide the reader an introduction to the work described in the following chapters of this document. The context is identified as well as the objectives and the author's motivation. Section 1.4 describes the document structure.

1.1 Motivation

Satellite miniaturization has been a challenge for applications, like Synthetic-Aperture Radar (SAR), that use these platforms and require high gain antennas. The antenna gain is directly related to its reflector size, in terms of wavelength. Therefore, in order to use high gain antennas, a large reflector is needed. However, these antennas are dimensionally inadequate, large and heavy, to be accommodated in such satellites. To overcome this, the proposed solutions have been evolving towards the use of deployable antennas. One deployment technique is to inflate an antenna.

Inflatable antennas are showing a growing interest for space related missions due to their portability, lightweight and its ratio between stowed and deployed volumes. They can be used in applications where having conventional reflectors is impractical or expensive. Within this context, the SARIA experiment has emerged and successfully applied to BEXUS, a segment of the REXUS/BEXUS programme, which gives the opportunity to university students to fly their experiments on stratospheric balloons. SARIA aims to perform SAR of the ground surrounding the flight path, from the BEXUS gondola, using an inflatable antenna and a Commercially Available Off-The-Shelf (COTS) Software Defined Radio (SDR). SARIA is a student project in which the author has been involved in since its beginning, 2019. The choice of this dissertation topic was only natural for the author, as it allows to continue the work carried out until now.

1.2 Context

The SARIA experiment is expected to fly onboard the BEXUS 31 gondola which typically reaches the stratosphere at altitudes from 25 km to 33 km during a flight of 2 h to 5 h. SARIA will look to perform SAR of the ground surrounding the flight path, from the BEXUS gondola, using an

inflatable antenna and a COTS SDR. Furthermore, a COTS parabolic reflector will also be used to create SAR images, for comparison purposes. These antennas will operate at 5.8 GHz. The experiment functional diagram is shown in figure 1.1 and includes the following subsystems:

On-Board computer Performs data handling of the samples captured by the SDR. Also performs several control and telemetry tasks, and is connected to the BEXUS E-Link system.

SDR board and RF frontend This subsystem is responsible for generating and transmitting the RF signals that will be used by the SAR technique, and then performing the data collection of the respective echoes.

Antennas This subsystem is composed by an inflatable antenna and a COTS parabolic reflector. Prior to a SAR session, one of these antennas is selected by the RF frontend in order create a SAR image.

Pressure control system Continuously monitors the pressure inside the inflatable antenna and performs inflation or deflation, as needed.

Navigation system Comprised of a Global Positioning System (GPS) and an Inertial Measurement Unit (IMU), measures the heading, position and velocity of the gondola.

Cameras Are responsible for capturing the inflatable antenna state and the ground flown by the BEXUS gondola.

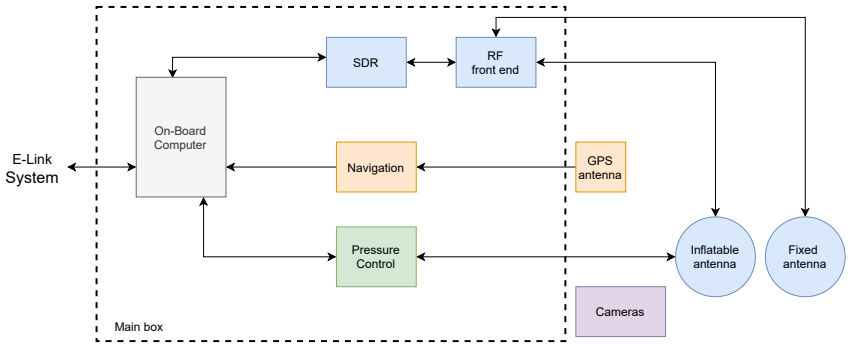

Figure 1.1: SARIA functional diagram

In the ground station, there is a computer connected to the BEXUS E-Link, that is able to communicate with the experiment on board. It will be able to download telemetry (eg. navigation data) and to issue commands such as “Inflate antenna now”. It will also be able to download SAR data and to display, in real time, both telemetry and generated images. There will also be another computer, this one connected to the internet, in order to show a map with telemetry data overlaid, allowing SARIA to decide when to perform a SAR session. SARIA main subsystems will be housed in a main box which is placed inside the BEXUS gondola, as seen in figure 1.2. Outside this main box, there is a boom, designed to hold the inflatable antenna, a COTS parabolic reflector, two cameras, and a GPS antenna.

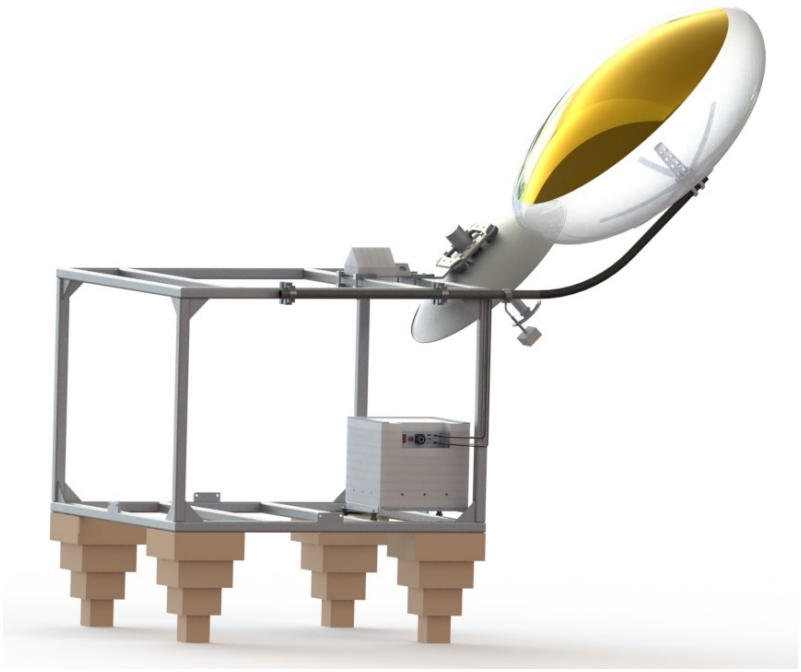

Figure 1.2: SARIA experiment assembled in the BEXUS gondola, credits: SARIA

The author has been directly involved in the pressure control system and in the inflatable antenna, which makes SARIA highly related to this dissertation work. Being SARIA a large student project it involves the contribution from other students. Two other dissertation works, from Gonçalo Santos [1] and Tiago Martins [2], are focused on the subsystems *On-Board computer, navigation, SDR board and RF frontend*. Nuno Barros is responsible for SARIA mechanical systems design and assembly. Gonçalo Xavier and Nuno Schumacher for the ground station software and Bernardo Moreira has contributed for the integration of the experiment.

1.3 Objectives

The main objective of this dissertation work is to contribute to the development of an Inflatable Parabolic Reflector Antenna (IPRA) for SARIA which will be used as one of the antennas to perform SAR. This antenna, with a diameter of 1 m, should be operational at 5.8 GHz and its differential pressure controlled using an active inflation system. Simulation will be used to obtain the IPRA inflated shape in order to determine its optimal differential pressure and characterize its RF properties. An inflatable antenna will be manufactured, characterized and compared to a dish antenna and simulation results.

1.4 Thesis structure

This thesis is organized in six chapters. The current chapter has introductory purposes. In the following chapter, the problem addressed by this thesis is presented as well as the proposed approach

to solve it and the state of the art. The third chapter contains the description about the design and manufacturing of the inflatable antenna whereas the fourth chapter includes a characterization of the pressure control system. Chapter 5 describes the executed tests and respective results. In chapter 6, conclusions and future work are presented.

Chapter 2

Overview

This chapter focus on describing the problem, section 2.1, addressed by this thesis and the proposed solution to solve it, section 2.2. Moreover, the last section of this chapter, 2.3, gathers the work developed by different authors.

2.1 The problem

The SARIA experiment, selected to fly in a stratospheric balloon in the scope of the REXUS/BEXUS programme cycle 13, consists in performing low-power SAR with a SDR using an inflatable antenna. Until now, SARIA has not been able to develop an operational Inflatable Parabolic Reflector Antenna (IPRA). Two antennas were developed, however they suffered from considerable air leakage and wrong material thickness selection, resulting on a relatively heavy antenna. Furthermore, these antennas RF properties have never been measured, preventing the assessment of its design. A tool is needed to assist on the initial developing phases of the IPRA, evaluating its RF properties at several differential pressures prior to the manufacturing phase. Additionally, this tool should be able to determine the IPRA optimal differential pressure interval. The IPRA shape is dictated by the differential pressure the IPRA is subject to. Theoretically, this shape will reach a perfect paraboloid, however studies have shown that this is not possible. Meaning, IPRA surface inaccuracy will exist and the overall antenna performance will be less than the one predicted. Tuning the differential pressure of the IPRA allows to adjust the IPRA shape. By finding the optimal differential pressure of an IPRA it is possible to minimize the RF gain loss due to surface inaccuracy. Optimizing the inflation pressure is seen as an improvement of the inflatable antenna overall performance [3, 4, 5]. The problem this thesis addresses is to determine the differential pressure interval which allows to take full advantage of an IPRA RF performance.

2.2 The approach

The development cycle of an IPRA can be divided in three phases: design, manufacturing and testing. In the design phase, the IPRA inflation, using different pressures values, will be simulated

using a commercial available FEA software, *Abaqus/FEA* . This simulation will give an estimate, at different inflation pressures, of the final IPRA shape that is obtained from its initial configuration. The IPRA simulated reflector surface is, then, imported to a *Matlab* script which computes the RF radiation pattern of such surface. This combination will allow to assess the RF properties of an IPRA design and identify the optimal differential pressure interval. The main objective of this approach is to reduce time in the developing phases of an IPRA and give confidence a certain IPRA design will perform well before the antenna is manufactured. In the manufacturing phase, state of the art COTS materials will be selected for the IPRA. Moreover, the antenna will be assembled by hand with the help of wooden molds. Finally, in the testing phase, the assembled IPRA RF properties will be measured and compared to simulation results and to a dish antenna.

2.3 State of the art

An Inflatable Parabolic Reflector Antenna (IPRA) is a closed body inflated by gas, maintained at a certain pressure, with the purpose to achieve the same functionalities as a fixed reflector antenna. Inflatable structures designed as parabolic reflectors have been a subject of interest for several years now. Parabolic reflectors typically have high directivity gains and are sought by applications with such requirement. The IPRA structure is typically obtained by joining together a reflector and a canopy. RF transparent material is used on the canopy and a metallized material on the reflector: Mylar®, a thin membrane material, is normally selected since it is RF transparent and reflective when metallize [6]. By using thin membranes, an IPRA, compared to a fixed reflector antenna, has lower weight, higher storage efficiency, and is cheaper to manufacture [7, 8, 9]. These IPRA properties make it very attractive for numerous space and earth applications.

The first experiment involving an inflatable antenna, *Echo 1* [10], was conducted by the NASA Langley under Project Echo. *Echo 1*, figure 2.1, was balloon shaped with a diameter of 30.48 m and was made using 12.7 µm thick Mylar® with vapour-deposited aluminium. This experiment, a first of its kind, successfully deployed, in space, an inflatable antenna which operated as a passive reflector. *Echo 1* was launched on 12th August 1960 and remained on Earth orbit until May 1968. As a passive reflector, it allowed for worldwide communications by retransmitting signals to Earth [10]. Project Echo launched into space another balloon, *Echo 2*, on 25th January 1964, re-entering the atmosphere on 7th June 1969. *Echo 2* is larger than *Echo 1*, with a diameter of 41 m, and has a rigidizable membrane. It was used as a passive experiment testing platform for communications. Moreover, *Echo 2* was used for global geometric geodesy [11].

Figure 2.1: Echo 1 ground inflation test, credits: NASA

The Inflatable Antenna Experiment (IAE) consisted of deploying in space an inflatable antenna based on L'Garde, Inc. concept study and technology advancements in this area [8, 12]. It was successfully deployed after being launch on 19th May 1996 aboard the Space Shuttle STS-77, figure 2.2. The IAE used an inflatable torus and strut to support the inflatable reflector [7]. The inflatable antenna configuration was a 14 m diameter parabolic reflector and was made using 62 aluminized Mylar® gores with a 6.35 µm thickness. An inflation system was used to control the pressure of the inflatable antenna based on L'Garde designs [12]. The gas source was high pressure nitrogen and the pressure control elements included valves, regulators and sensors. The deployment on orbit and inflation of the torus and strut was successful, however the complete inflation of the reflector was not accomplished because the deployment sequence did not go as planned: the amount of residual air was greater than expected inside the inflatable structures [13].

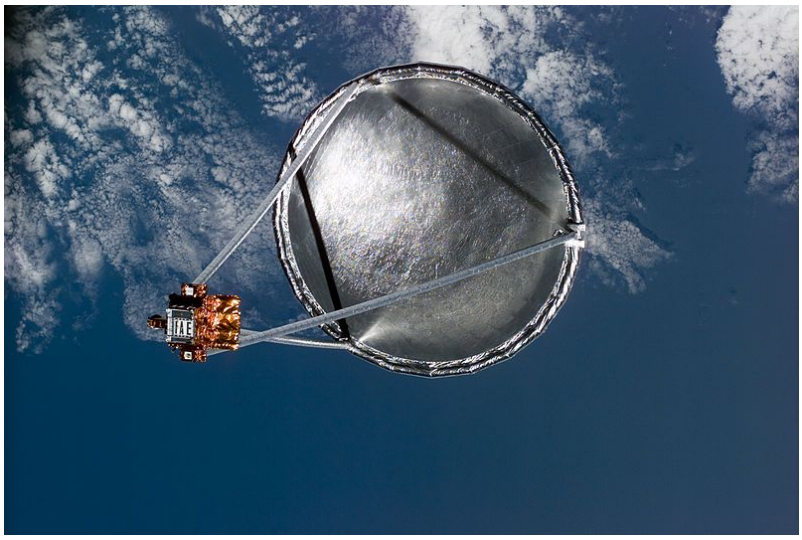

Figure 2.2: Release of the IAE, credits: NASA

Project Echo [10] and the IAE [13] remain, until date, the only space demonstrations of inflatable antennas, having greatly contributed for the development of the inflatable antenna concept and technology advancements. Nevertheless, new inflatable antenna designs and analysis methods have been proposed since then. Manufacturing and design phases of inflatable antennas are a source of errors which downgrade its RF performance. The problems that designers face involve surface and shape accuracy, optimal pressure, leakage and selected materials, for example. During the operational phase, the antenna pressure should be stable and sufficient enough to maintain the antenna RF performance at its maximum.

Robert A. Hoferer and Yahya Rahmat-Samii, 1998, present a new design entitled "inflatable radiometer imaging system" which is a combination of inflatable antenna technology and a "parabolic torus reflector antenna" [14]. Furthermore, for this antenna design, the authors characterise a distortion model, capable of predicting the antenna RF characteristics when operating. Tan et al., 2011, study the surface accuracy of an inflatable antenna with a 3 m diameter by varying the inflation pressure [15]. In this work, a photogrammetry software is used to measure the surface accuracy. The authors concluded, in order to improve the inflatable antenna surface accuracy, the inflation pressure should be defined considering the amount of surface wrinkles (to be minimized) and the Root Mean Square (RMS) surface value. It was observed that this last property increased with the increase of the inflation pressure and a great part of surface errors originates from the edges and centre of the reflector [15]. Yan Xu and Fu-ling Guan, 2012, developed analysis methods used to calculate the initial shape of a reflector surface and the gores shape [3]. In this study, a 3.2 m inflatable antenna reflector was designed and manufactured using the proposed analysis, the antenna pressure was maintained at 20 Pa, using ambient air as gas source. A photogrammetry system was used to test the reflector surface accuracy, which was less than 1 mm RMS [3]. Wang Hong-jian et al. , 2012, have designed and tested a 3 m inflatable antenna with a lenticular structure and small f/D, [4]. The authors compared the inflatable antenna RF performance on the L-,C- and X- bands. The surface accuracy error was 0.98 mm, determined using a photogrammetry testing technique.

Under the Inflatable Antenna for CubeSat Project [16], several inflatable antenna designs have been studied and proposed in which an inflatable antenna is to be stored and deployed on a CubeSat. Babuscia et al., 2013, have detailed a first design of an inflatable antenna to operate at the S-band with a reflector diameter of 1 m, [17]. Two inflatable antenna shapes (cylinder and conical) are proposed and compared using results from simulations: the cylinder shape (simulated peak gain of 21 dB) performed better than the canonical shape (simulated peak gain of 16 dB) [17]. Although both of the proposed shapes did not achieved a "perfect parabolic shape", when inflated on a vacuum chamber test, the initial shapes were obtained. Sublimating powder (benzoic acid) was selected to be used as a passive inflation agent. Radiation tests results, at an anechoic chamber, show the cylindrical shape has similar experimental and simulated gains, whereas the conical shape experimental gain was lower than the simulated gain [17]. The authors believe this difference was caused by a possible air leakage. Design wise, an initial non-inflated parabolic antenna will tend to a spherical shape when inflated, not converging into a parabolic shape [18,

19]. Thus, to obtain an inflated parabolic shape, the initial non-inflated shape is not necessarily an ideal paraboloid [18]. Another inflatable antenna prototype designed to operate at the X-band is described in [18], 2016, with an estimate gain of 34 dBi. Two designs for the initial shape were proposed: "an undersized curved paraboloid surface" and an "entirely flat" surface [18]. The objective of these initial surfaces was, when inflated, they would tend to an approximate parabola. An empirical test approach was chosen to analyse the effects of pressure on the antenna shape. To characterize both inflated shapes at different pressure values, each one was subject to a photogrammetry test where the antenna pressure was manually controlled. The flat surface presented less wrinkles and better approximated a parabola when inflated. For this reason, it was selected for testing in order to validate its RF gain simulations: peak gain was 24.7 dBi and directivity peak was 24.9 dBi . During the RF measurements, a pressure control system was used, providing the option of using different inflation pressures. The authors were able to find a pressure value which stabilize the antenna for an 8 h scan, allowing the reflector to have the same profile during RF measurements. Measurements show the peak directivity was 24.2 dBi and an antenna gain of 19.4 dBi, this difference might be a consequence of the patch antenna used [18]. With this RF test, the authors were able to show that the proposed design is able to have a similar performance as a rigid reflector, "given the right pressure conditions" [18]. In [19], 2017, a new spherical design for an inflatable antenna is described in order to increase the X-band gain of the prototype presented in [18].

The performance of a reflector parabolic antenna is influenced by its geometry. To obtain a manufactured parabolic surface with the same gain as the one designed is rather difficult since there are several random sources of errors present on the manufacturing and assembling phases of a parabolic antenna [20]. These errors will produce what is called a random surface deviation and it is characterized by the RMS surface error. A consequence of this surface deviation is the appearance of phase errors which negatively impacts the projected antenna gain [20]. Ruze [21] derived an equation, 2.1, which relates the directivity gain loss with the RMS surface error for small phase errors. Ruze assumes these errors have a *Gaussian* distribution.

$$\frac{G}{G_0} = e^{-\frac{4\cdot\pi\cdot\varepsilon}{\lambda}^2} \tag{2.1}$$

$\frac{G}{G_0}$ = normalized gained loss

ε = RMS surface error

λ = wave length

Welch, 2006, demonstrated the Ruze equation is not applicable to assess the RF performance of "inflatable large aperture antenna" [22]. In his work, RF measurements were performed to determine the directivity gain of an inflatable antenna (offset inflatable aperture antenna) at six different pressures, using ambient air. As well as photogrammetry tests, in the same conditions, were performed to obtain the inflatable antenna RMS surface error. The measured directivity

gain values were subtracted to the simulated gain, this difference is called by the author as "RF-Derived Surface Loss", and were compared to the "Ruze-Derived Surface Loss" at each pressure level used. Results show the Ruze equation "overstated the directivity degradation" since the inflatable antenna shape dominant errors are not uniformly distributed as the ones contemplated in the Ruze equation. On an inflatable antenna the non-uniform surface errors are due to the existence of wrinkles, when it is under inflated, and the fact the inflatable antenna will not reach a perfect paraboloid surface when inflated [22]. Furthermore, different pressure values produced different directivity gains. Following this finding, a mathematical model is proposed by Welch, 2019, to obtain an inflated surface of an "inflatable large aperture antenna" in order to provide a mean to characterize it [9].

Fenn et al., 2019, present an inflatable antenna design and manufacturing approach, "axisymmetric array-fed confocal parabolic Gregorian reflector antenna", for space applications using small satellites. The authors manufactured an inflatable antenna prototype and characterize it at the X-band [23, 24]. The measured peak directivity is 37.6 dBi at 10 GHz and the simulated peak directivity is 41.4 dBi.

The use of finite element analysis software is widely spread in engineering nowadays. This type of software programme solves problems using the FEM analysis: subdividing a system into a finite number of elements from which an approximate solution for partial differential equations is obtained [25]. Furthermore, it is capable of simulating the behaviour of simple and complex systems under different situations. Palisoc and Yuli developed a finite element software, *Finite Element Analysis of Inflatable Membranes (FAIM)*, to analyse deformations in inflatable antennas and inflatable solar concentrators, [26], and combined it with a group of existing software programmes in order to have a tool set capable of analysing and designing such structures. Furthermore, the authors managed to alter one of these programmes, an RF antenna code, into accepting the nodal coordinates of a FAIM simulated inflatable antenna surface,[26] , with the purpose of evaluating its RF parameters. There are several software programmes commercially available which can be used to simulate the inflation of structures: *Abaqus Unified FEA*, *LS-DYNA*, *Kangaroo Physics*. Chandra et al. have used *LS-DYNA* to simulate the shape of a Ka-band inflatable antenna after inflation [27]. In this work, wrinkle analysis is performed on the resulting inflated surface and it identifies three distinct regions divided by the amount of wrinkles present. In particular, the "wrinkle free region" has demonstrated to be feasible for RF applications using the Ka-band. In addition, the authors calculate the RMS error of the simulated inflatable antenna surface which is then used to compute the expected gain with respect to an ideal parabolic surface with different f/d ratios, in the Ka-band.

Inflatable antenna applications can also be found on Earth. GATR Technologies has successfully developed terrestrial inflatable antennas. Currently, there are four commercially available models of different sizes and operate at "Ku-,C-,X- and Ka-bands"[28]. One of GATR inflatable antenna models, currently available, is shown in figure 2.3. These antennas have been used in emergency response, severe weather situations and by the military.

Figure 2.3: GATR 4.0 Antenna System [29]

Naomi Mathers presents and characterizes an inflatable antenna design to operate at the Ku-band in terrestrial conditions: under the presence of gravity, atmosphere pressure and extreme weather conditions [5]. The objective of this work is to prove an inflatable antenna can achieve the same RF performance of an identical fixed rigid antenna under the mentioned conditions. The proposed design is a "dual reflector" obtained from a primary and secondary reflectors, and a conical feed horn which are manufactured using Polyethylene Terephthalate (PET) thin film [6, 5]. The used components were manufactured as an inflatable and as a fixed structure for comparison reasons and the used frequency for RF simulations and measurements was 12.5 GHz. Results obtained by Mathers using the inflatable antenna manufactured, figure 2.4 (a prime focus antenna with a diameter of 0.5 m), demonstrate it is possible to manufacture an inflatable antenna from thin membrane materials and achieve good RF performance under gravity conditions.

Figure 2.4: Mathers' inflatable antenna under RF measurements, [5]

Differential pressure is the means by which the inflated inflatable antenna shape is obtained. This inflation pressure will directly influence the inflatable antenna RF performance. To calculate the operational pressure values needed to maintain the antenna shape, Mathers uses two equations which provide a lower and an upper limit of the desired operational pressure interval [5]. The lower limit is identified as the one in which wrinkles are eliminated from a material after deployment. This happens when the stress level in the Mylar® is 6.89 MPa [7, 5]. The appearance of wrinkles on an antenna surface degrades its accuracy since it contributes to alter the final inflated shape [15, 18]. The upper limit is determined by the material used with the least yield strength. Operating at pressures above this limit will result in a deformed shape, deteriorating the inflatable antenna performance. The optimal pressure value, the one which will allow to obtain the most accurate antenna shape, resides within this inflation pressure interval [5]. Sublimating powder, for example benzoic acid, can be used as a gas source to inflate an antenna, avoiding the use of active inflation systems. In space applications, these type of powders are widely used due to the absence of a permanent gas source and other constraints [17], for example mass budget. In this thesis, sublimating powder will not be used as a gas source since, first, chemical calculations are not under this thesis scope, and, second, there is an unlimited gas source: air. With this, an active inflation system will be used to control the pressure of the inflatable antenna. From here onwards, the active inflation system will be referred as pressure control system.

The pressure control system is composed by a controller unit, pressure sensor, air pumps and valves. Its objective is to maintain the pressure of a certain system at a target pressure level or interval. Pressure control systems are present in a variety of applications and industries. In healthcare, pressure control systems can be found in blood pressure monitoring devices or electronic ventilators, for example. In the automotive industry, pressure control systems are used to inflate tires automatically. In the field of soft robotics, pressure control is being used at low level control to accomplish complex robotic tasks [30]. Several hobbies and open source projects are available online in which pressure control systems are implemented using COTS components.

Chapter 3

Design

This chapter is divided into five sections. The first one details the IPRA design. The second one describes how the IPRA inflation simulation is implemented as well as how its RF properties are computed. Furthermore, the antenna dimensions and materials are identified and the simulation results are presented. The last three sections describe how the antenna is manufactured and assembled.

3.1 Design description

As mentioned, the SARIA experiment will be housed in the BEXUS 31 gondola. This platform, figure 3.1a, dimensions are 1.16 m x 1.16 m x 0.84 m, [31]. In addition, besides SARIA, it will house three other experiments. The IPRA, with a diameter of 1 m, is going to be mounted to a boom, secured to the BEXUS gondola according to figure 3.1b. With this set up, the boom ensures the IPRA is tilted at 45° NADIR and illuminates, figure 3.2 , a swath of a few km situated about 30 km to the left or right of the gondola flight path.

(a) BEXUS gondola during a launch campaign, credits: REXUS/BEXUS programme

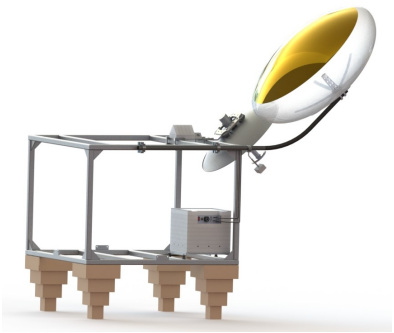

(b) IPRA mounted to the SARIA boom credits: SARIA

Figure 3.1: BEXUS gondola overview

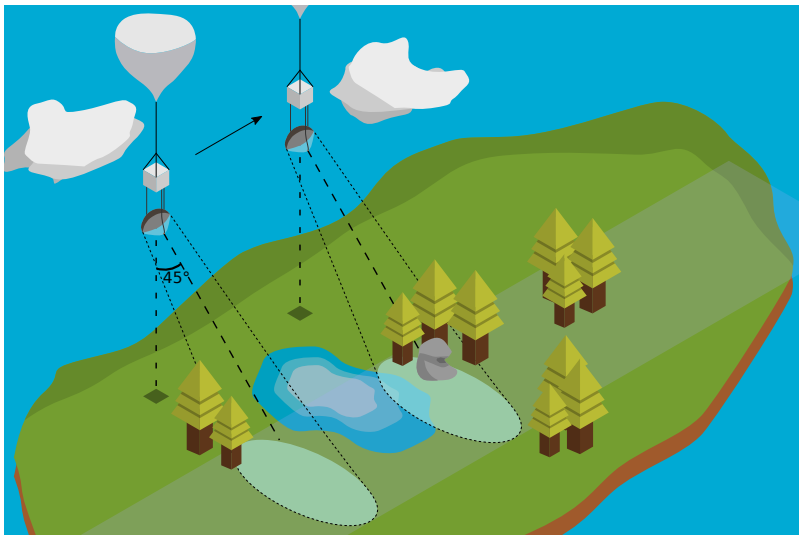

Figure 3.2: Mid-flight representation of the SARIA experiment (not to scale). While represented hanging from the gondola, the antenna will instead be supported by a boom, credits: SARIA

The IPRA is a closed body obtained from joining two parts, a reflector and a canopy, with the objective to achieve the same functionality as a fixed reflector antenna. The initial inflatable antenna configuration will influence its final inflated shape.The proposed design, figure 3.3, is a combination of one parabola and two ellipses. The antenna reflector part, highlighted in green, is formed by a parabola and an ellipse. The antenna canopy, highlighted in blue, is a single ellipse. Ellipses are used to ensure the IPRA shape is maintained when inflated. From here onwards, the reflector part will be referred to as top part and the canopy as bottom part. To manufacture the corresponding 3-dimension model, 360° revolution about its axis, the principle described in [32] is used. The authors describe how to build a paraboloid from derived 2-dimension buds. This same method can be applied to manufacture ellipsoids.

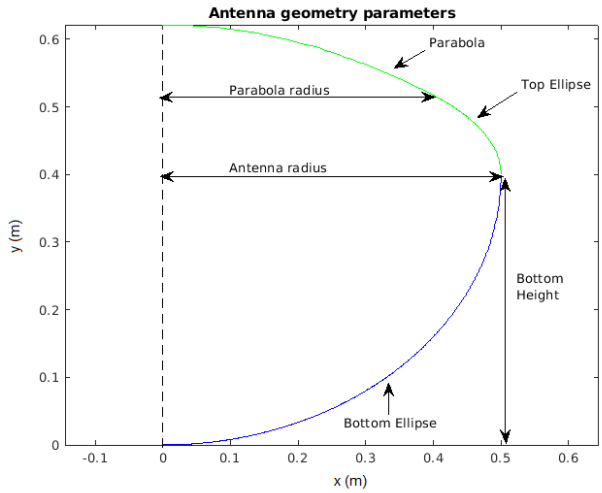

Figure 3.3: Proposed inflatable antenna design curves, vertical cut view

The parabola is obtained using the same mathematical formula used for static parabolic reflectors, equation 3.1. Both ellipses are computed using the mathematical formula 3.2. By varying, R_x and R_y, different ellipses are obtained. A constraint is, at the junction parabola-ellipse, its equations must have the same derivative to ensure curve continuity.

$$y = \frac{x^2}{4 \cdot f} \tag{3.1}$$

$f =$ feed focal length

$$\frac{x^2}{R_x^2} + \frac{y^2}{R_y^2} = 1 \tag{3.2}$$

Three geometry parameters (*parabola radius, antenna radius, bottom height*) are identified in figure 3.3 and have a direct impact on equations 3.1 and 3.2. Different geometry parameters, will produce distinct curves which results in a different antenna design. The *parabola radius* will affect directly the parabola curve, the *antenna radius* and *parabola radius* the top ellipse, the *bottom height* and *antenna radius* the bottom ellipse. Taking these parameters into consideration equations 3.1 and 3.2 are rewritten as follows.

Figure 3.4 identifies several parameters used to calculate the focal length of a parabola. The distance, r_f, between a point in the parabola and the focal length, f, for a given feed angle, θ_f, is computed using equation 3.3, [33].

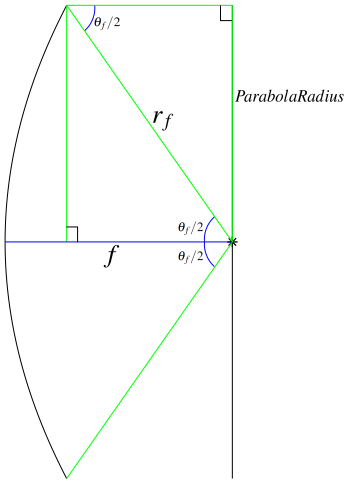

Figure 3.4: Parabola parameters identification

$$r_f = \frac{2 \cdot f}{1 + \cos(\theta_f/2)} \tag{3.3}$$

For a point at the end of the parabola, $r_f = \frac{ParabolaRadius}{\sin(\theta_f/2)}$, the focal length, f, for a given feed angle, θ_f, becomes:

$$f = \frac{ParabolaRadius \cdot (1 + \sqrt{\tan^2(\theta_f/2) + 1})}{2 \cdot \tan(\theta_f/2)} \tag{3.4}$$

Using equation 3.4, the parabola curve is defined by equation 3.5.

$$y = \frac{x^2}{4 \cdot \frac{ParabolaRadius \cdot (1+\sqrt{\tan^2(\theta_f/2)+1})}{(2 \cdot \tan(\theta_f/2))}} \tag{3.5}$$

$\theta_f =$ feed angle
$x \in [0, ParabolaRadius]$

The top ellipse R_x is equal to the *antenna radius* and R_y is obtained using equation 3.8 at $x = ParabolaRadius$. It is calculated by equalling the equations 3.6 and 3.7 that correspond to the derivatives of equations 3.1 and 3.2, respectively. The top ellipse is obtained using equation 3.9.

$$\frac{\partial y_{parabola}}{\partial x} = \frac{x}{2f} \tag{3.6}$$

$$\frac{\partial y_{ellipse}}{\partial x} = \frac{-R_y \cdot x}{R_x \cdot \sqrt{R_x^2 - x^2}} \tag{3.7}$$

$$R_y = -\sqrt{R_x^2 - x^2} \cdot \frac{R_x}{2f} \tag{3.8}$$

$$y = -\sqrt{AntennaRadius^2 - x^2} \cdot \frac{\sqrt{AntennaRadius^2 - ParabolaRadius^2}}{2 \cdot f} \tag{3.9}$$

$f =$ focal length
$x \in [ParabolaRadius, AntennaRadius]$

The bottom ellipse R_x is equal to the *antenna radius* and R_y to the *bottom height*. Its formula is described by equation 3.10.

$$y = \sqrt{AntennaRadius^2 - x^2} \cdot \frac{BottomHeight}{AntennaRadius} \tag{3.10}$$

$x \in [0, AntennaRadius]$

3.2 Simulation

The inflatable antenna RF performance will depend on the differential pressure used to maintain the antenna inflated. It is important to determine a differential pressure range since it will define the IPRA shape and how accurate its reflector surface is, allowing to take advantage of its full RF performance. A way of determining the differential pressure interval is empirically, where the antenna is assembled, the pressure is varied and the RF gain is measured. However, this process is not the most efficient for testing different designs: first, it requires an abundance of material and human resources, and, second, it is time consuming since assembling each design by hand takes

time. The method proposed by the author is to simulate the inflation sequence and compute the radiation pattern of the resulting IPRA reflector surface, allowing to quickly assess the IPRA RF performance. This gives confidence in proceeding to the assembling of an IPRA design, reducing time and money on less accurate designs.

Simulating the antenna inflation requires the use of a finite element analysis software, in this work *Abaqus/FEA* was used. The FEM problem is determining the shape to which the IPRA will tend at several differential pressure values. Being electrical and computers engineering the author background, FEM and the use of FEM analysis tools are topics the author was unfamiliar with. Thus, this work does not focus on the fundamentals of FEM analysis of the IPRA, but on taking advantage of this tool as a mean to obtain an inflated reflector surface from which the antenna radiation pattern can be determined. This is achieved by using a *Matlab* script which imports the inflated reflector from *Abaqus/FEA* and computes its radiation pattern. *Abaqus/FEA* is a unitless programme, therefore the user must carefully define the values provided to *Abaqus/FEA*, it was decided all values were passed using the International System of Units (SI) system.

3.2.1 Antenna dimensions

With the proposed design method to obtain the initial antenna configuration, section 3.1, there is a large number of possible antenna designs to choose from. One of SARIA requirements is the antenna shall have a total diameter of 1 m, limiting the IPRA *antenna radius* to 0.5 m. This makes it possible to change two parameters: the *parabola diameter* and the antenna *bottom height*. In order to make the parabola curve, equation 3.5, only dependent on the *parabola diameter*, the feed angle was fixed at 110°. After running several simulations with different parameters values using an ideal inflatable antenna model, its initial configuration is obtained by making a 360° revolution of the parabola and ellipses curves about its axis, the *parabola diameter* was fixed at 0.78 m and the *bottom height* at 0.38 m. Also, it was decided both the antenna top part and bottom part are divided in 8 segments (buds). This decision is a trade off between manufacturing complexity, weight of the seams material and antenna closeness to its design curves. If the number of antenna buds increases, the antenna tends more to the desired shape. However, the material quantity needed to seam the different buds also increases. This contributes to increase the overall antenna weight and its construction complexity.

3.2.2 Material selection

Metallized COTS Mylar® has been selected for the IPRA top part since it must be made from RF reflective material. Contrary, the IPRA bottom part must be made from RF transparent material, thus COTS transparent plastic has been selected. To join the different antenna elements Kapton® is used. These choices were made based on the available literature, in which these materials have been used in similar applications. The Kapton® tape is considered to have a width of 2 cm for the simulated model. On *Abaqus/FEA*, the following material properties were used:

Table 3.1: Material properties used in *Abaqus/FEA*

Material	**Density** (kg/m^3)	**Young Modulus** (Pa)	**Poisson Ratio**	**Thickness** (m)
Mylar®	1390	3.500×10^9	0.38	13×10^{-6}
Plastic	904	1.325×10^9	0.43	30×10^{-6}
Kapton®	1420	2.500×10^9	0.34	55×10^{-6}

3.2.3 Method

The following figure 3.5 describes the simulation flow used to evaluate the chosen geometry parameters, from designing the antenna to simulating its inflation and computing the resulting radiation pattern. Furthermore, it can be used for any value of IPRA geometry parameters. Ultimately, this simulation approach will give an estimate of the expected antenna gain as well as the differential pressure interval that guarantees it and the feed focal length (relative to the final inflated reflector surface). One of *Abaqus/FEA* features is the possibility to sketch a certain part. However, for the IPRA it has revealed to be rather difficult since there is no option to sketch a parabola, for example. A combination between a *Matlab* script and *Abaqus/FEA* to design the antenna was adopted. A second *Matlab* script is used to compute the antenna radiation pattern. Another *Abaqus/FEA* feature is the ability to run scripts written in python. When using the *Abaqus/FEA* graphical interface, it records the user session, translating it into a python script, saved in a file known as replay file. By consulting this file and the *Abaqus Scripting Reference Guide*, [34], a general python script was developed which automates repetitive tasks in *Abaqus/FEA* when preparing the IPRA model to be submitted for simulation.

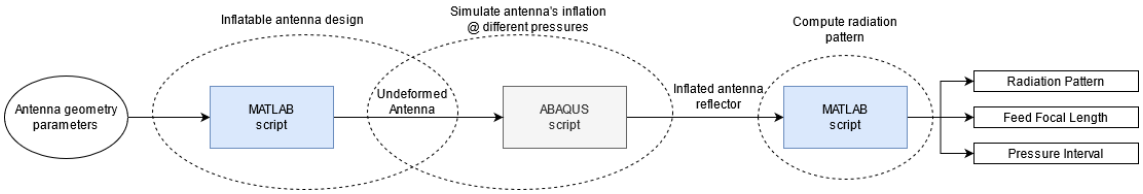

Figure 3.5: IPRA simulation flow

3.2.3.1 Description

Figure 3.6 shows a high level block diagram of the developed *Matlab* script to design the IPRA parts: top and bottom. The IPRA is manufactured from planar buds which means its initial configuration is not an assembly of a perfect revolution of parabolas and ellipses, as considered previously. The following IPRA 3D bud model, figure 3.7a, is generated: the lateral edges of each bud, alternated coloured lines, are computed using the IPRA design equations and the rest of the bud surface is obtained by computing the meridians between this edges, lines in green and blue. The angle between each coloured lateral edge is 45°, which corresponds to 360° divided by the total number of buds (8). One way of exporting these parts, top and bottom, to *Abaqus/FEA* is by means of an *.stl* file. This requires the points generated in figure 3.7a to be converted into a

Matlab surface. In order to do so, the *Matlab* function *scatteredInterpolant* is used with its interpolation method defined as *linear* and its extrapolation method as *nearest*. The resulting parts to be exported to *Abaqus/FEA* are shown in figures 3.7b and 3.7c. To convert these surfaces to a *.stl* file the function *stlWrite* from [35] is used with the *mode* set as *ascii* and the *triangulation* as *"Forward slash division of grid quads"*.

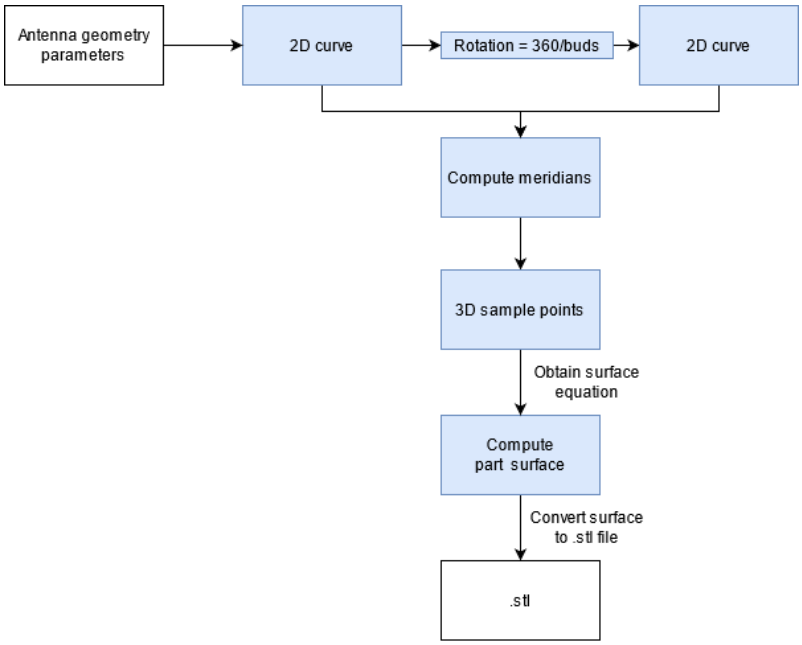

Figure 3.6: *Matlab* script to create the top and bottom part of the IPRA initial configuration

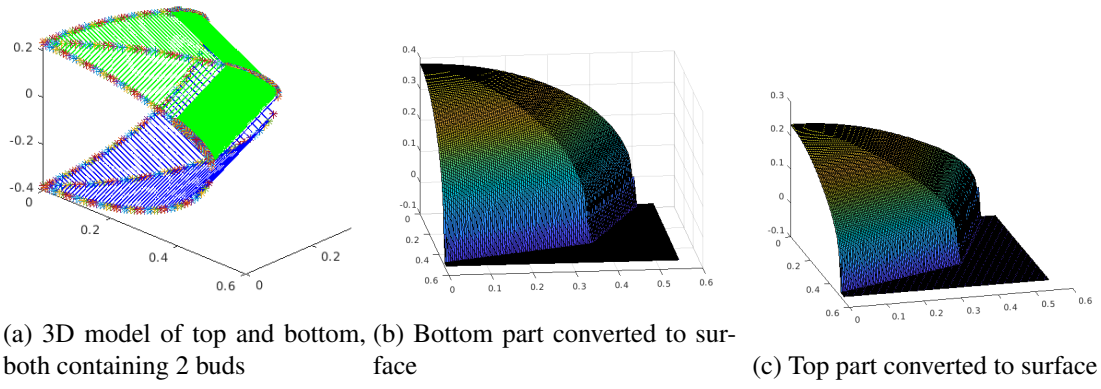

(a) 3D model of top and bottom, both containing 2 buds

(b) Bottom part converted to surface

(c) Top part converted to surface

Figure 3.7: *Matlab* part design

After the parts are designed in *Matlab*, they are imported by the *Abaqus/FEA* script, which high level block diagram is shown in figure 3.8. The step procedure used in *Abaqus/FEA* is *Dynamic,Explicit*.

Before obtaining the parts to assemble the antenna in *Abaqus/FEA*, several steps are necessary to ensure that the parts are correctly imported, figure 3.9. Either the bottom and the top part *.stl* files, figure 3.9a, are converted and imported as *.igs* file. Allowing to have the two parts in the same

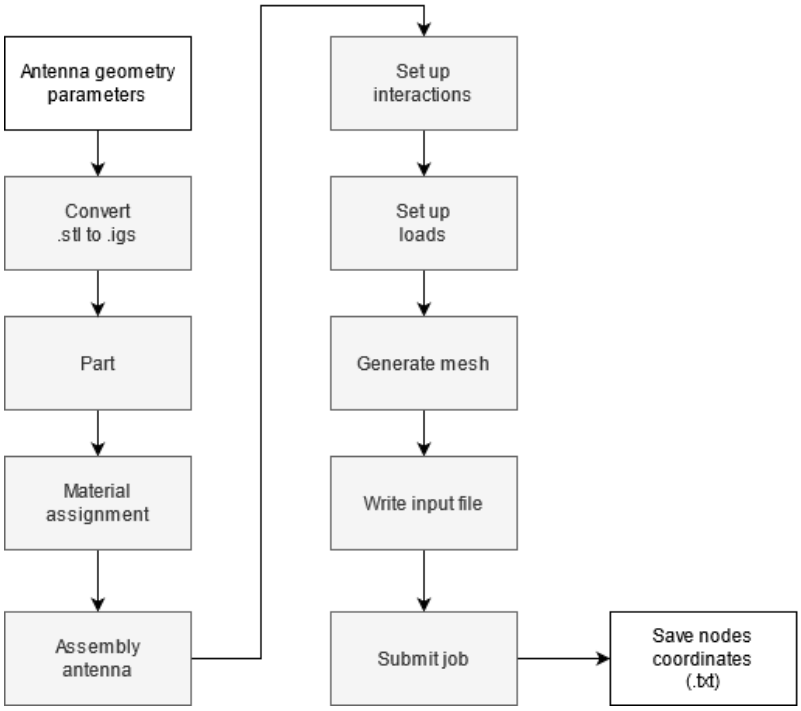

Figure 3.8: *Abaqus/FEA* script block diagram

Abaqus/FEA model. The following step is to remove the bud which became deformed, figure 3.9b and 3.9c , and, after, mirror the non-deformed bud, figure 3.9d, forming the top/bottom part which will be used to assemble the antenna. Once the parts are obtained, the materials are assigned to them according to figure 3.10 and the material properties are described in table 3.1. Following this, the IPRA is assembled by instantiating the bottom and top parts, figure 3.11. *Tie constraints* are defined to tie the instantiated part edges in order to form a closed body in *Abaqus/FEA*.

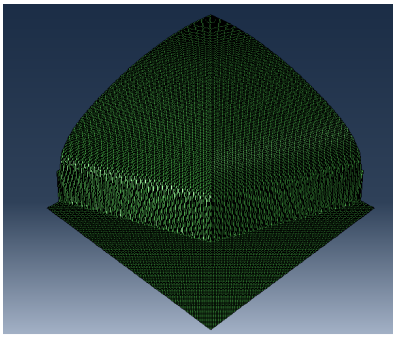

(a) An *.stl* is imported into *Abaqus/FEA*

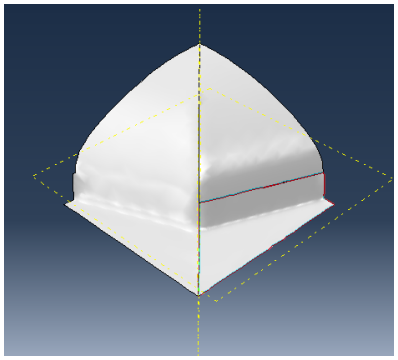

(b) The *.stl* is converted into an *Abaqus/FEA* part and partitioned

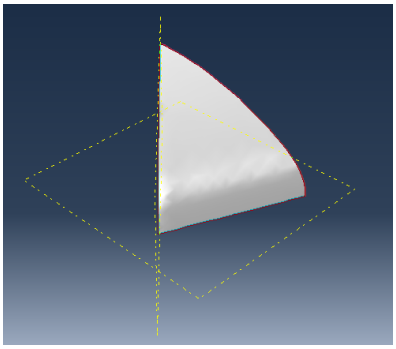

(c) Bud extraction

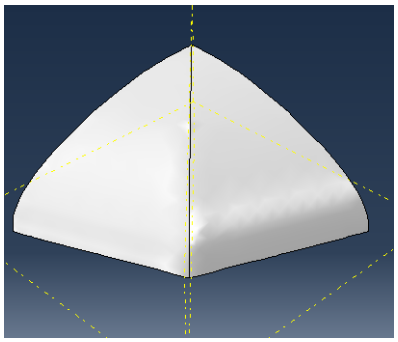

(d) Mirror bud

Figure 3.9: Conversion of an imported *Matlab* part to a *Abaqus/FEA* part, a quarter of the antenna is shown

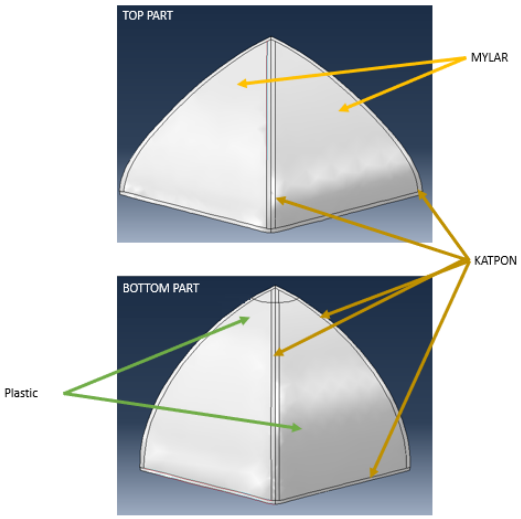

Figure 3.10: Material assignment

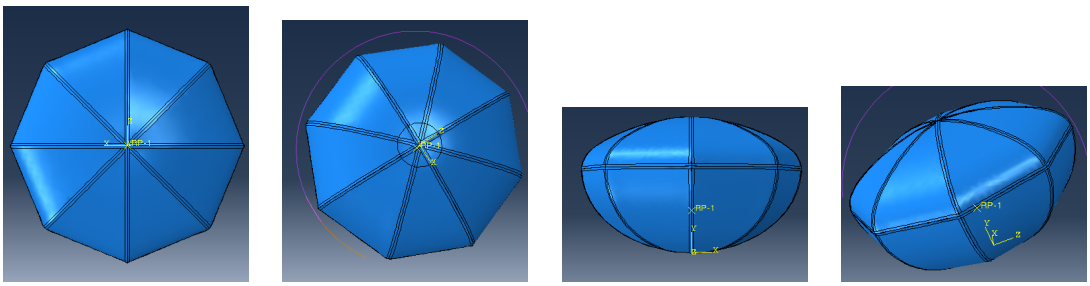

(a) Top view (b) Bottom view (c) Front view (d) Side view

Figure 3.11: Assembled IPRA model

The simulation is composed by a total of 52 steps. The first step, *Remove_Volume*, is used to deflate the initial antenna configuration, with visualization purposes. The subsequent odd steps, *pxxx*, are used to inflate the antenna from 100 Pa to 2500 Pa, where *xxx* represents a differential pressure value. On the even steps, *No_LoadsX*, no loads are applied to the model, allowing to visualize its behaviour after applying a certain load. Table 3.2 summarizes the simulation steps as well as each step time.

Table 3.2: Simulation step description

Step number	Step name	Time
1	Remove_Volume	0.15
2	No_Loads	0.05
3	p100	0.1
4	No_Loads1	0.05
...	...	0.1
...	...	0.05
51	p2500	0.1
52	No_Loads51	0.05

Two interactions are defined: **FLUID CAVITY* and **FLUID EXCHANGE*. The **FLUID CAVITY* is used to inform *Abaqus/FEA* the IPRA assembly is a volume filled by air at Mean Sea Level (MSL) ambient pressure. In this simulation, the **FLUID EXCHANGE* purpose is to allow air exchange between the fluid cavity and the environment, deflating the initial assembly. This option is latter deactivated at the simulation step number 2. The antenna will be fixed at its bottom by a circular part, to mimic this, the boundary condition *ENCASTRE* is applied to a set of bottom nodes, which limits all its degrees of freedom, figure 3.12a, which is a circumference with a radius of 9 cm. Gravity is added using the load type *Gravity* with a value of 9.81 m/s^2, figure 3.12b.

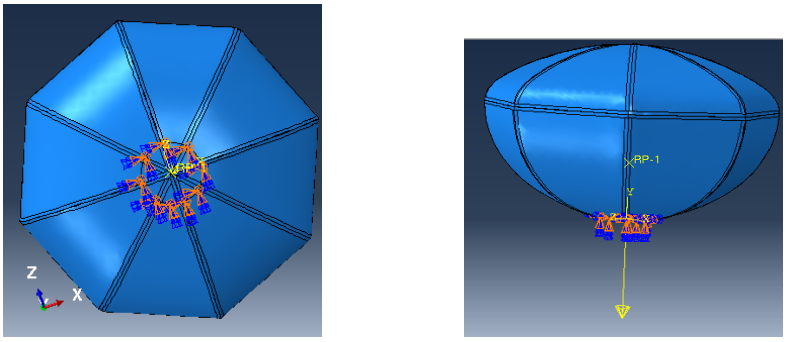

(a) Restricted bottom nodes (b) Gravity load

Figure 3.12: Simulation model load set up

In this *Abaqus/FEA* simulation, the differential pressure is set to vary between 100 Pa and 2500 Pa, spaced by 100 Pa intervals, using the boundary condition *Fluid cavity pressure*. After, the assembled antenna is meshed using the *global seed* tool, with the *approximate global size* set to 0.01, figure 3.13, the *Abaqus/FEA* input is written and the resulting job submitted.

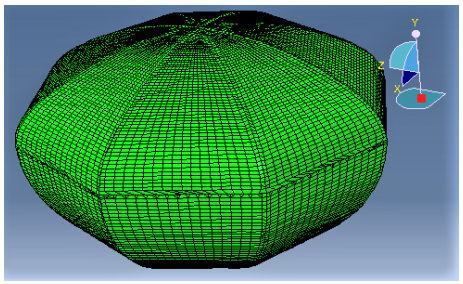

Figure 3.13: IPRA initial configuration, mesh size of 0.01

At the end of the simulation, the antenna top part nodes, figure 3.15a, are extracted from *Abaqus/FEA* output file and saved to a *.txt* file, writing the nodes X,Y and Z coordinates. It was defined the nodes were extracted from the last frame of each step the antenna model is subject to a new differential pressure load, odd numbered simulation steps. These last frames correspond to differential pressures between 100 Pa and 2500 Pa, spaced by 100 Pa intervals. To process this data, a second *Matlab* script was developed and its high level block diagram is shown in figure 3.14.

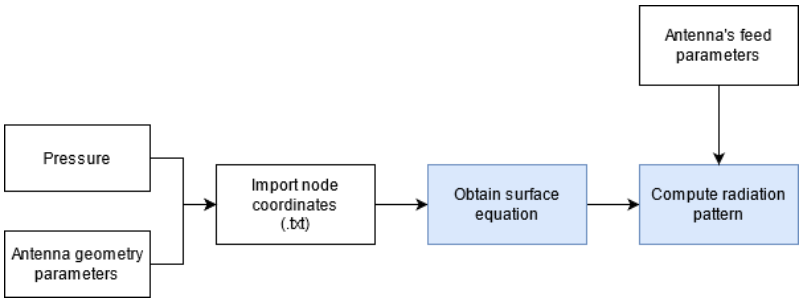

Figure 3.14: *Matlab* script block diagram to compute the radiation pattern of an IPRA

According to the desired differential pressure value and antenna geometry parameters, the corresponding *.txt* node file is imported. With this X,Y and Z sampled data, the antenna top part (reflector) is recomputed in *Matlab* using the function *scatteredInterpolant*, figures 3.15b and 3.15c. The interpolation method was defined as *linear* and the extrapolation method as *nearest*. The resulting antenna surface equation is used to obtain the deformed reflector, figure 3.15d, allowing to compute its radiation pattern for a given antenna feed. This is done using a *Matlab* script based on the following principle: the antenna reflector surface is divided into elementary planar segments which are considered to be small enough to irradiate equally to all sides. For each element, the received energy area from an incident wavefront is calculated as well as phase delays. After, the obtained values are summed coherently. This *Matlab* script was developed prior this dissertation work and was modified into accepting different antennas surfaces. The selected IPRA feed is a 5.8 GHz patch antenna, figure 3.16, designed by [36], its gain is 7.5 dBi and its beamwidth at -3 dBi is 70°.

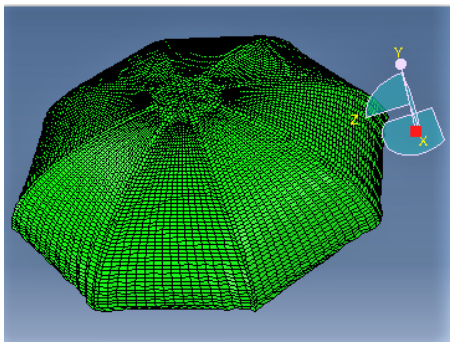

(a) *Abaqus/FEA* visualization of IPRA deformed top green)

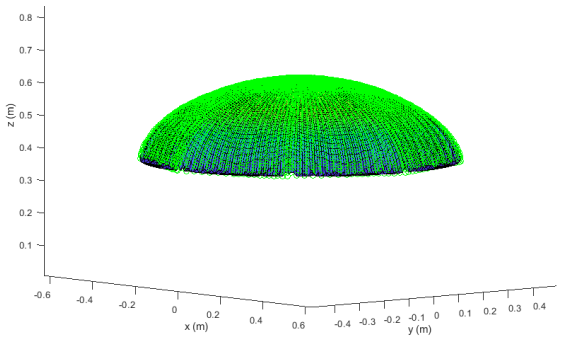

(b) Surface computation using sampled nodes (in

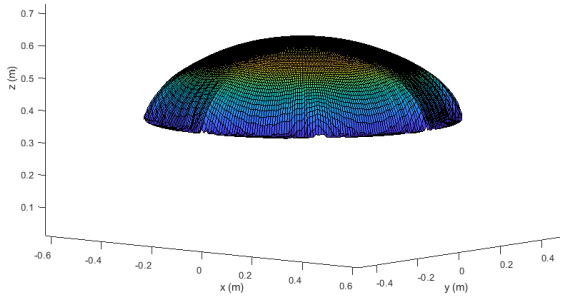

(c) Reflector surface computation without extracted nodes

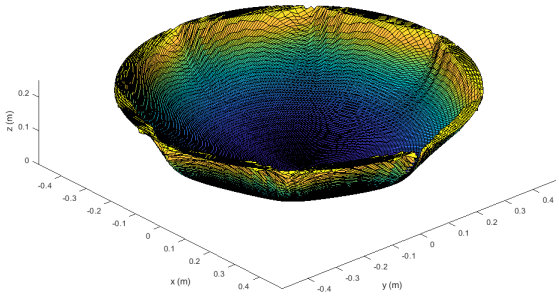

(d) Reflector surface used to compute radiation pattern

Figure 3.15: From node extraction to reflector surface computation, visualization for a differential pressure of 1000 Pa

(a) Patch antenna made from dielectric material

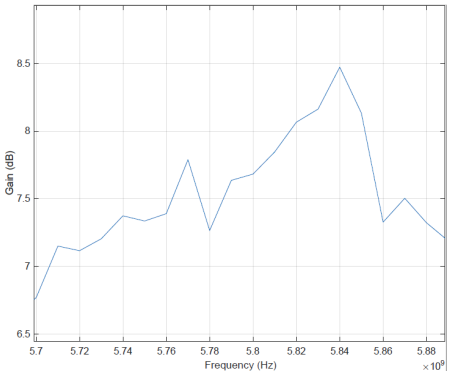

(b) Measured gain of the patch antenna

Figure 3.16: Patch antenna properties, credits: [36]

3.2.4 Results

The IPRA differential pressure and volume throughout the simulation are shown on the *Abaqus/FEA* history graph, figure 3.17. *Abaqus/FEA* is a unitless programme and the values shown are in SI units as mentioned previously. The volume change in the IPRA with the differential pressure increase is approximately 10 L , when the differential pressure starts rising the volume is at 284 L and, at the maximum simulated differential pressure, is at 294 L. The IPRA deformed shape after inflation is shown in figure 3.18.

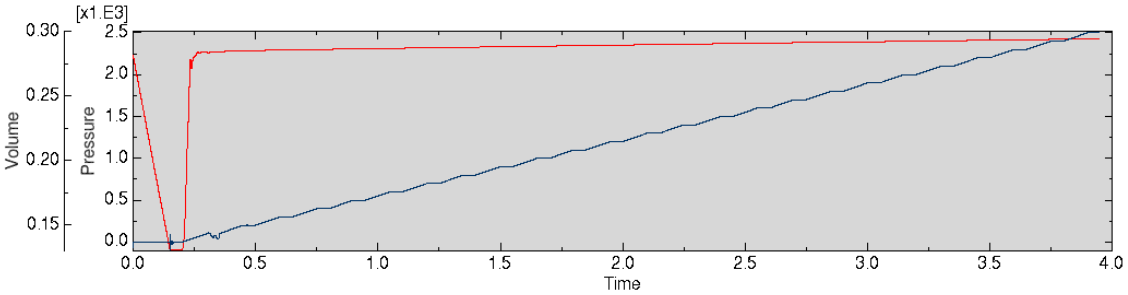

Figure 3.17: IPRA volume change (in red) and IPRA differential pressure load (in black), SI units

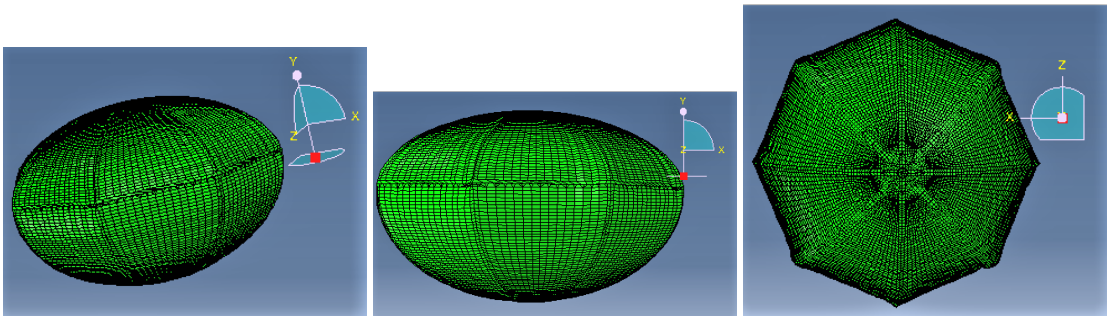

(a) Front view (b) Side view (c) Top view

Figure 3.18: Visualization of IPRA inflated with 1000 Pa of differential pressure

As seen in graph 3.17, there is some initial instability on the IPRA volume when the differential pressure rises from 0 Pa to 100 Pa, this translates to the antenna bouncing up and down when visualizing the results animation in *Abaqus/FEA*. On the next simulation steps, the volume and differential pressure stabilize. For this reason, another simulation was performed to obtain the inflated shape for 100 Pa without this instability. The radiation pattern is computed and the peak gain is extracted for the differential pressure interval of 100 Pa to 2500 Pa. The correspondent peak gains, at 5.8 GHz, for a certain differential pressure and optimal focal length are shown in figure 3.19b. These values were obtained using different focal lengths (0.3 m to 0.4 m) for the same reflector surface when calculating its radiation pattern.

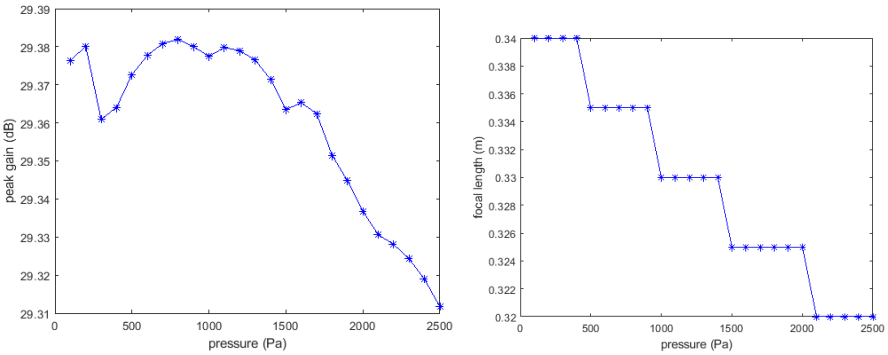

(a) Peak gains for different differential pressures

(b) Focal length for different differential pressures

Figure 3.19: Peak gain vs pressure for optimized focal length, considering the inflated reflector surface

The RF peak gains at each differential pressure value are shown in figure 3.20 for the three feed focal lengths 0.34 m, 0.335 m and 0.33 m. The antenna peak gain is sensitive to the differential pressure as well as the focal length used. This simulation result shows feed positioning, at different inflation pressures, influences the overall antenna performance. It is important to take special attention to the feed focal length once the antenna is manufactured and it should be adjusted accordingly to RF measurement tests results since the manufactured antenna may deviate from its initial configuration design.

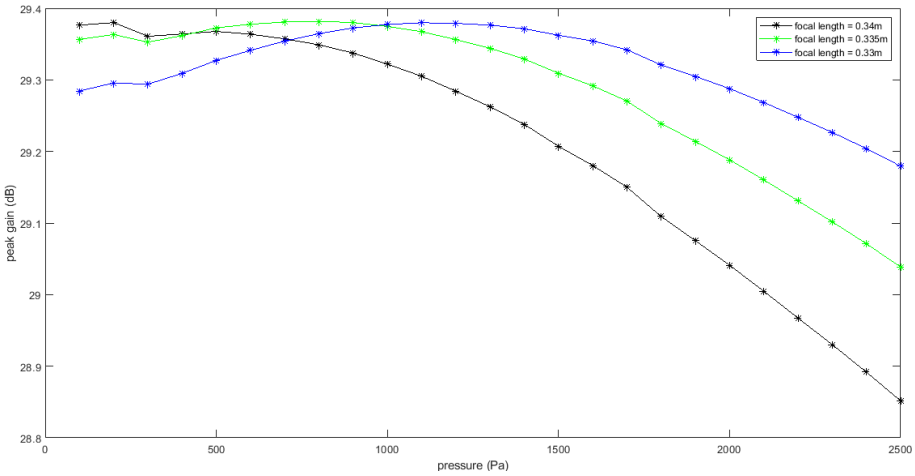

Figure 3.20: Peak gain vs differential pressure for different focal lengths at 5.8 GHz

As seen in figure 3.20, the optimal differential pressure interval, in which the maximum peak gain resides, varies with the focal length used. It is clear that for high differential pressure values (1.5 kPa to 2.5 kPa) the antenna performance degrades, since the maximum peak gains decrease, eliminating the necessity to inflate the IPRA to these differential pressures. Analysing the simulation results, the increase of the differential pressure, between 100 Pa and 1 kPa, does not significantly change the antenna RF gain, the variation is less than 0.2 dB for the same feed focal

length. This means with less differential pressure, 100 Pa, one can achieve the same RF gain as if using a differential pressure of 1 kPa. From this point of view, the optimal differential pressure interval is 100 Pa to 200 Pa, identified in table 3.3, for a focal length of 0.34 m, since it has the highest peak gain compared with the other focal lengths. The corresponding radiation pattern for each differential pressure is shown in figure 3.21. This simulation result provides an estimated differential pressure interval, peak gain and focal length. Manufacturing and testing a IPRA with the same dimensions used in this simulations will corroborate the obtained results.

Table 3.3: IPRA differential pressure interval and corresponding expected peak gain for a focal length of 0.34 m

Differential pressure (Pa)	**Peak gain** (dB**i**)
100	29.38
200	29.38

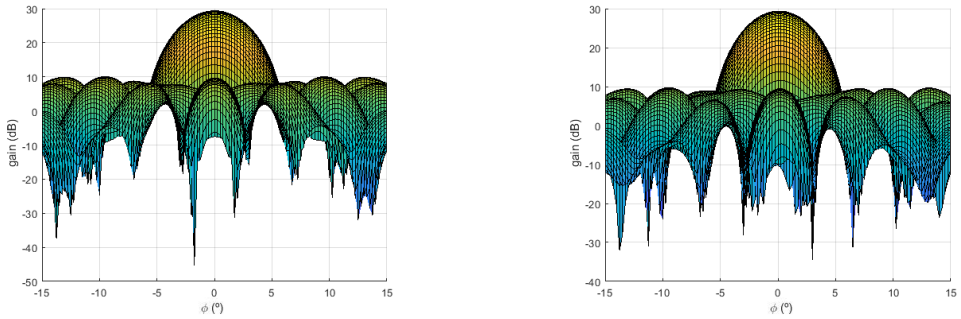

(a) Radiation pattern for a differential pressure of 100 Pa

(b) Radiation pattern for a differential pressure of 200 Pa

Figure 3.21: Radiation patterns for several differential pressures, with a focal length of 0.34 m

3.2.4.1 Comparison with an ideal parabolic reflector

The maximum gain of an ideal reflector is, [33]:

$$G_{max_{dBi}} = 20\log_{10}(\frac{\pi \cdot D}{\lambda}) \tag{3.11}$$

$D =$ antenna diameter

$\lambda =$ wavelength

Using equation 3.11, the gain of a parabolic reflector with a diameter of 1 m is 35.6 dBi, at 5.8 GHz. It is known that a reflector antenna has inefficiencies and typically the effective area, in terms of antenna gain, is approximately 50% (-3 dB) of the real aperture area, [33]. The main contribution for a reflector antenna inefficiency is the feed radiation pattern not being uniformly distributed over the reflector plate. This means the feed concentrates more of the irradiated power

in the reflector centre instead of in the reflector periphery. By irradiating the reflector plate periphery less, the feed takes little advantage of the periphery and energy is lost to the outside of the reflector plate. Considering a 50% inefficiency, the gain of a parabolic reflector with a diameter of 1 m becomes 32.6 dBi.

The radiation pattern and peak gain of a perfect parabolic antenna was computed by the previously used *Matlab* script. This parabolic antenna, figure 3.22, has the same diameter as the IPRA, 1 m, and is illuminated by the same antenna feed, [36]. The antenna peak gain, at 5.8 GHz, for different focal lengths is shown in figure 3.23.

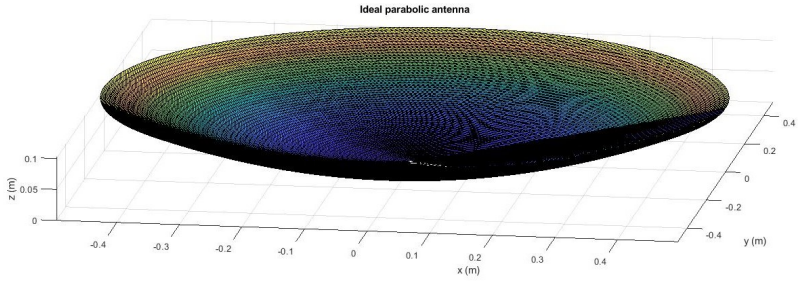

Figure 3.22: IPRA ideal parabolic curve, reflector diameter of 1 m

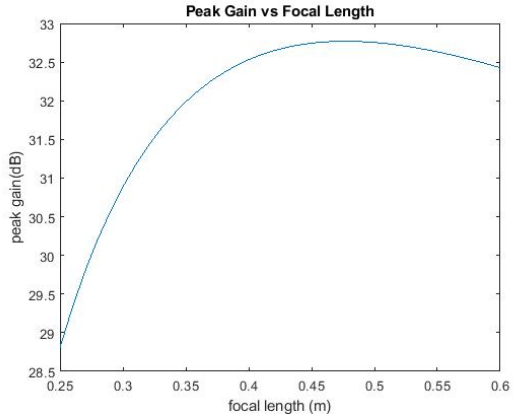

Figure 3.23: Antenna gain vs focal length for a reflector diameter of 1 m at 5.8 GHz

For an ideal parabolic antenna with a diameter of 1 m and optimal focal length of 0.48 m, the peak gain is 32.77 dBi. This result from the *Matlab* script is in line with the predicted -3 dB gain loss due to antenna inefficiency. This *Matlab* script takes into account the feed radiation pattern and the losses of the feed itself, it is made from dielectric material. Nevertheless, it considers the metal of the parabola to be a perfect reflector with no losses. Typically, the reflector is not a perfect conductor and, therefore, has losses when reflecting. This is almost residual: a maximum loss of 0.5 dB.

The parabola of the IPRA has been designed with a diameter of 0.78 m. Comparing to a reflector with a diameter of 0.78 m, the IPRA gain should be 30.5 dBi (50% of efficiency). However, the maximum calculated gain, section 3.2.4, is 29.38 dBi. The IPRA reflector, diameter of 1 m,

is made of a parabola and an ellipse. Meaning the ellipse addition and the inflation process itself will deviate the IPRA parabolic reflector from the desired parabolic shape. Consequently, the antenna feed is no longer optimized since it was designed to illuminate a parabolic reflector with a diameter of 1 m for a specific f/d. This change in the reflector shape has, thus, contributed to a gain loss of 1.12 dB. Nevertheless, the use of an ellipse facilitates the reflector construction method. This result demonstrates the proposed IPRA design will not reach the same performance as a paraboloid reflector antenna. Gain loss is expected to exist when this antenna is inflated. The accumulation of errors which inevitably happen during the manufacturing phase of the IPRA will also contribute to RF performance loss. Therefore, it is expected the IPRA gain to be lower than the estimated one.

3.3 Antenna construction and assembly

Ideally, the bonding of IPRA buds would be carried out by a specialized professional company in this matter. However, due to the experimental nature of an IPRA, such professional expertise currently does not exist in the author geographical location. With this, the IPRA is assembled by hand, adding human error to the IPRA initial configuration assembly. Nevertheless, a manufacturing procedure was carried out in order to minimize this error. The IPRA dimensions are described in section 3.2.1 with the top and bottom part having a total of 8 buds each. The buds were designed with a *Matlab* script following the principle described in [32] which can be applied to paraboloids and ellipsoids. The top part buds, composed by a paraboloid and an ellipsoid projection, are shown in figure 3.24c which is a combination of figures 3.24a and 3.24b. The bottom part buds, composed by an ellipsoid projection, are shown in figure 3.25a.

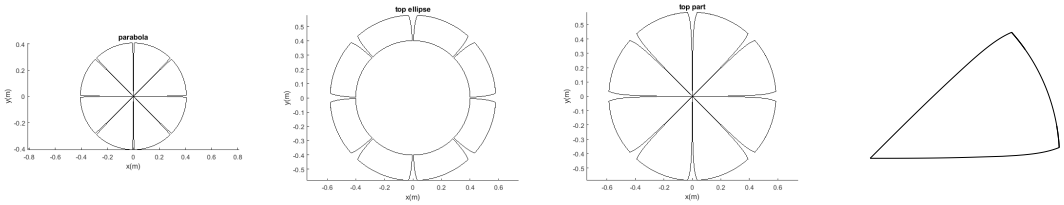

(a) Parabola projection (b) Ellipse projection (c) 8 buds (d) Single bud

Figure 3.24: *Matlab* IPRA top buds design

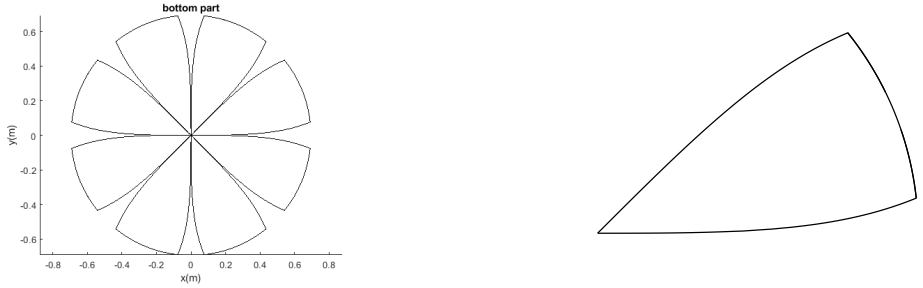

(a) 8 buds (b) Single bud

Figure 3.25: *Matlab* IPRA bottom buds design

Single buds are extracted from the top and bottom part, 3.24d and 3.25b respectively, and wooden molds are created from it, figures 3.26a and 3.26b. These molds are used to cut 8 buds from Mylar® (top buds) and plastic (bottom buds) with thickness identified in table 3.1. To facilitate the antenna assembly, using these flat buds, three other wooden molds are created, figure 3.26c. To give the IPRA top part and bottom part buds its design curvatures described in figure 3.3, the molds 3.26d and 3.26e are created, respectively. The third wooden mold, which corresponds to the rounded curve of a single bud, is shown in figure 3.26f and it is used to assist in joining together the top and bottom part.

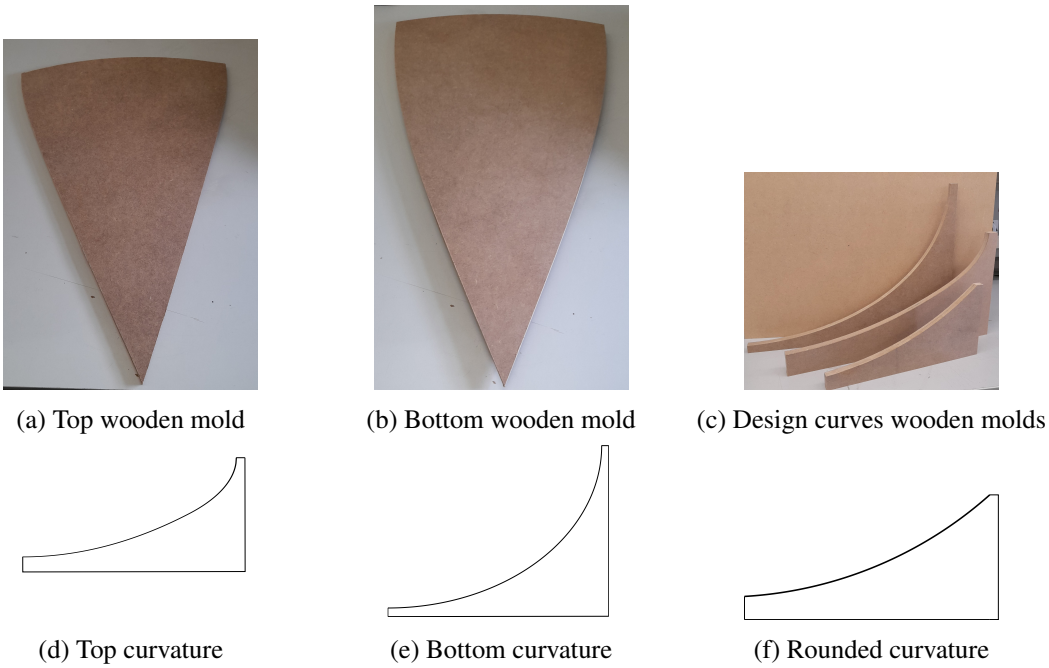

(a) Top wooden mold (b) Bottom wooden mold (c) Design curves wooden molds

(d) Top curvature (e) Bottom curvature (f) Rounded curvature

Figure 3.26: Molds used to assist on IPRA assembly

To join together the several flat buds, double sided Kapton® tape with a 5 mm width is used to juxtapose the cut buds. Firstly, the Kapton® tape is fixed to the wooden mold which has a guiding line, figure 3.27a. Secondly, the buds are positioned and placed on the Kapton® tape, figures 3.27b and 3.27c. Thirdly, a second Kapton® tape , with a 5 mm width, is placed to provide more resistance and minimize air leakage, trapping the juxtapose section between these two Kapton® tapes, figure 3.27d. Furthermore, Kapton® tape with a 8 mm width is placed over the double sided Kapton® tape to fulfil two purposes: to prevent the different antenna buds from sticking to each other and minimize air leakage. The following assembly order is repeated until the IPRA is constructed, figure 3.27f:

1. Creation of pairs of juxtaposed top buds.
2. Creation of pairs of juxtaposed bottom buds.
3. Juxtaposition of the resulting pairs (top and bottom), figure 3.27e.
4. Juxtaposition of the obtained pairs, Mylar® first and, then, plastic, without closing the last plastic pair.
5. A circle (10 cm diameter) is cut out on the centre of the IPRA top part and replaced by a smooth Mylar® circle, using Kapton® to fixate it.
6. Antenna closure, to auxiliary the last plastic juxtaposition, a circle (9 cm diameter) is cut in the bottom part, creating enough space to place one hand inside the IPRA.

(a) Double sided Kapton® is fixed to a wooden mold

(b) Plastic bud is placed over the Kapton® tape following a guiding line

(c) Mylar® bud is placed over the Kapton® tape following a guiding line

(d) After two buds are juxtaposed, another Kapton® tape is placed on top of it

(e) Juxtaposition of the top and bottom pairs

(f) IPRA assembled

Figure 3.27: Different IPRA manufacturing stages

3.4 Antenna mounting

On its end application, the IPRA will be fixed to a boom which is bent 45°. In order to guarantee the IPRA will not move out of place once tilted 45°, a circular support part is fixed to the bottom of the antenna. This piece diameter was obtained after running a simulation on *Abaqus/FEA*. The antenna model used is the same one used in the section 3.2, with a higher *global seed*, 0.065, decreasing the total computation time. This simulation simulated the IPRA behaviour when tilted 45° under the presence of gravity and subjected to a differential pressure of 1000 Pa. The circular part was modelled by the boundary condition *ENCASTRE* which was applied to a circumference set of bottom nodes similar to figure 3.12a. The radius of this circumference was increased until the IPRA no longer moved out of the central position. On the first steps of the simulation, no loads were applied, so only the effect of gravity was present. Next, the antenna is inflated to the target differential pressure, and, after, no loads are applied. The behaviour of the IPRA was analysed by inspecting the simulated *Abaqus/FEA* animation. In figure 3.28a, with a diameter of 20 cm, the antenna still moves to its sides. The original position is shown in transparent and the displaced antenna in blue. However, with a diameter of at least 24 cm, figure 3.28b, the antenna is able to stay on the intended position.

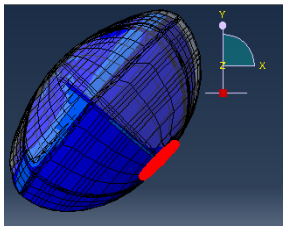

(a) Circumference node set with a 20 cm diameter

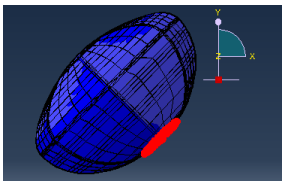

(b) Circumference node set with a 24 cm diameter

Figure 3.28: Antenna displacement simulation

As mentioned above, the antenna support was designed taking into consideration the *Abaqus/FEA* simulation result. To add a safety margin, the diameter of this part was defined to be 28 cm. Figure 3.29a shows the interface between the antenna and this support. And, figure 3.29b shows the support attached to the IPRA. This support was designed with the help of Nuno Barros and 3d printed by an external company.

(a) Interface between the support and the IPRA

(b) Support attached to the bottom of the IPRA

Figure 3.29: Inflatable antenna back support

3.5 Feed placement

From the simulations results obtained in section 3.2.4 it was possible to conclude the feed focal length must be adjusted once RF tests are performed as it is highly dependent of the final inflated surface. The feed height is the distance between the antenna feed and the boom holding the antenna. Increasing this height will decrease the feed focal length and vice-versa. A modular feed support piece, figure 3.30b, composed by parts with different heights, figure 3.30a, was designed, again, with the help of Nuno Barros and 3d printed by an external company. The goal of the feed support piece is to adjust the feed height during RF tests. The maximum possible feed height is 36 cm and the minimum feed height is 15.5 cm. The selected IPRA feed is a 5.8 GHz patch antenna developed by [36].

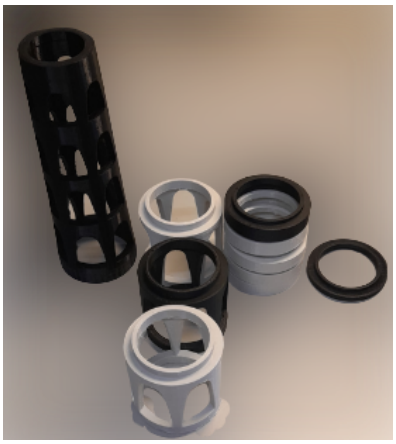

(a) Modular feed pieces

(b) Feed placed on its support

Figure 3.30: Feed support

Chapter 4

Pressure control system

The aim of this chapter is to describe the implementation of the pressure control system. In section 4.1, a characterization of the chosen hardware is made. The last section, 4.2, contains the details about the developed software to control the pressure inside the IPRA.

4.1 Hardware

The inflatable antenna is inflated using ambient air and controlling the pressure inside the antenna is a critical part since it directly influences the IPRA RF performance as described in section 3.2.4. The pressure control system block diagram is shown in figure 4.1.

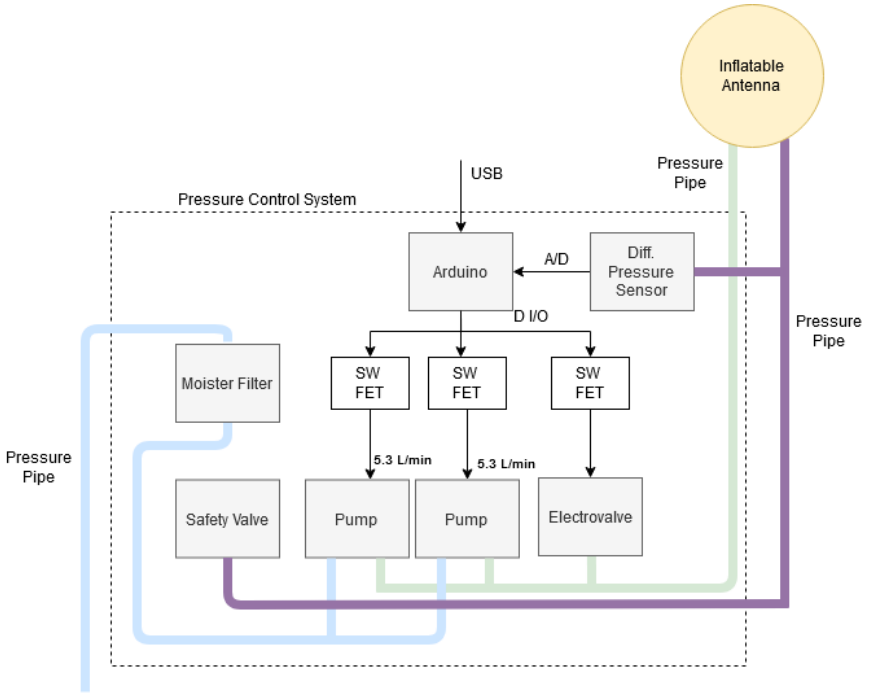

Figure 4.1: Pressure control system block diagram

The IPRA pressure is monitored by a differential pressure sensor. The goal is to maintain this differential pressure between a desired interval, in which the IPRA shape is stable and its gain is maximum, by actuating on the electronic valve and pumps. A total of three pipes are used. One for air intake (in blue), one for differential pressure monitoring (in purple), and another to pump or remove air of the IPRA (in green), see figure 4.1. The reason a separate pipe is used to monitor the IPRA differential pressure is the actuation of the pumps can lead to spikes in the pipe air pressure, which would cause the differential pressure sensor to misread the IPRA pressure or, even, result in sensor damage. The same reason justifies the connection of the safety valve to the pressure monitoring pipe. Furthermore, with this configuration, the differential pressure sensor is capable of detecting if the safety valve is operating or not. These last two pipes are connected to the IPRA from SARIA main box and each has an approximate length of 3 m.

The pressure control system elements inside the dashed rectangular of figure 4.1 are shown in an existing pressure control Printed Circuit Board (PCB) designed to host the mentioned hardware. The pumps and electronic valve actuation is based on Field Effect Transistor (FET) drivers. The following subsections present the selection of the pressure control system components which was made taking into consideration they are going to be used in SARIA, experiencing a low pressure ambient.

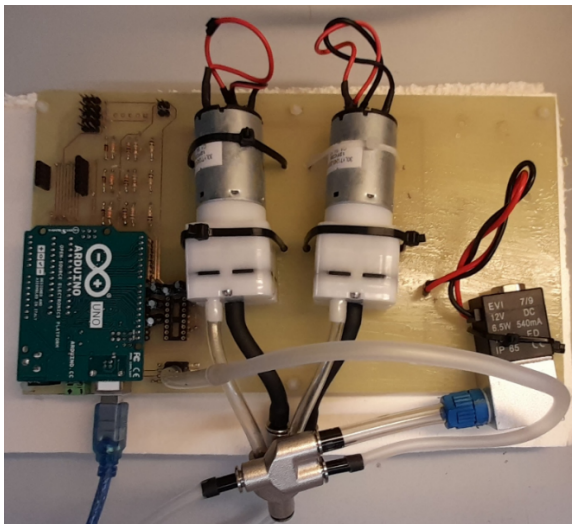

Figure 4.2: Pressure control system pcb

4.1.1 Controller unit

The controller unit is responsible for making decisions, whether or not pump air into the antenna, based on the IPRA differential pressure. For this, it has to be able to read data from sensors and drive actuators. Microcontroller Units (MCUs) are the most appropriate embedded devices to use in this type of applications. Nowadays, the MCU industry has a great deal of MCUs available. The *Arduino Uno* is a low cost, low complexity and easy to programme MCU board which uses the ATmega328p MCU from Microship. The mentioned characteristics make the *Arduino Uno* a very

attractive and popular MCU among developers, existing a large support community, justifying its selection as the MCU for the pressure control system. There is no need for a more complex one since the *Arduino Uno* specifications meet the system requirements.

4.1.2 Air Pumps

Air pumps are used to blow air into the IPRA, inflating it. An important characteristic of air pumps is its volumetric flow rate expressed in l/min. The air compressors commercially available, for example to inflate a flat tire, with high volumetric flow rates are dimensionally inadequate (large and heavy) and its power consumption is high. Miniature air pumps are more adequate and widely used in smaller applications, for example in blood pressure monitoring devices. Diaphragm, rotary and rotary-diaphragm are three technologies available for air pumps.

The volume of the IPRA is expected to be circa 300 L and the antenna shall be inflated under 40 min upon the ascent phase of the BEXUS gondola to the stratosphere. Under these conditions, the minimum flow rate, necessary to completely inflate the IPRA, is 7.5 l/min. Nevertheless, air leakage is inherent to air pumps, so the air volume blown by it will be less than indicated by the manufactures. *35 RO-DV* rotary-diaphragm pump from Schwarzer Precision has a maximum volumetric flow rate of 5.3 l/min at MSL. One pump of this model is capable of filling a volume of 300 L in about 57 min, not considering leakage, which is not enough to meet the 40 min requirement. However, using two *35 RO-DV* pumps the maximum volumetric flow rate of 5.3 l/min increases to 10.6 l/min, filling a volume of 300 L in about 29 min, not considering air leakage. Since the atmospheric pressure decreases while the BEXUS gondola, where SARIA will be housed, ascends to the stratosphere, the residual air volume left inside the IPRA, prior to ascent, will expand and increase the IPRA pressure. Combining this passive inflation with the one provided by air pumps, the inflating time requirement can be met.

Pressure vessels are an alternative to air pumps to inflate the IPRA and are used to store a certain volume of a gas, generally, at pressures higher than ambient pressure. A typical BEXUS flight will reach an altitude of 25 km to 33 km during its float phase and ambient pressure will be around 10 mbar. As specified above the IPRA volume will be circa 300 L, considering a 85% pressure vessel inflation efficiency, the pressure vessel would need to supply approximately 350 L just to fill the IPRA. If the efficiency decreases, more volume is necessary. Since the IPRA and other pressure control elements may have air leakage, 350 L is not enough. Thus, an estimate of 600 L is sufficient to fill the IPRA under these conditions. However, if air leakage is greater than estimated, gas supply will run off, making it impossible to keep the antenna inflated. Increasing the pressure to which gas is subject to inside the pressure vessel, allows to store more gas using the same pressure vessel volume. The 600 L at 10 mbar can be supplied by a 3 bar pressure vessel with a 2 L volume. Which is a manageable volume, nevertheless, operating at this pressure value, or higher, carries safety risks and pressure reduction valves are needed, increasing the system complexity. The pressure vessel would also need to work under low temperatures experienced during a stratospheric flight. Moreover, comparing to miniature air pumps, for example the *35 RO-DV* model, pressure vessels are larger and heavier. All factors considered, even though pressure

vessels would be able to inflate the IPRA faster than air pumps, the overall risks and complexity increase do not justify its use. Also, if there is any problem with the antenna, a puncture for example, the air pumps are able to work continuously to compensate air leakage, contrary to pressure vessels since it only has a certain amount of gas available.

4.1.3 Pressure Sensor

Pressure, expressed in pascal (Pa), is the quotient between a fluid force and the surface area it is applied to. Devices used to measure this physics quantity are denominated as pressure sensors. Depending on the application, different types of pressure sensors are used: absolute, sealed gauge, gauge and differential [37]. Absolute pressure sensors are used to measure pressure referenced to vacuum and sealed gauge pressure sensors to measure pressure referenced to the atmospheric pressure. These two sensor types are used in applications where a constant pressure reference is needed. Gauge pressure sensors are used to measure pressure relative to a variable atmospheric pressure. Differential pressure sensors measure the difference between two arbitrary pressures. These two sensor types are used in applications where the reference pressure is variable. The most appropriate sensor type to use in the pressure control system is a gauge sensor since the IPRA internal pressure must stay the same, keeping a constant inflated volume, regardless of the ambient pressure. Being gauge pressure sensors the most common pressure sensor type, there are a large number of devices commercially available at different prices and from different manufacturers.

The performance of the pressure sensor is critical for a pressure control system, and it is influenced by the sensor range, resolution and its calibration. Poor pressure readings can lead to unexpected system behaviour, in the case of an IPRA, a poor pressure reading can make the control system over or under inflate it. Furthermore, a pressure sensor needs also to be reliable and robust. Pressure sensors with these characteristics are used in home appliances, for example washing machines (lifespan of around ten years), and are manufactured in large quantities, allowing for affordable prices. The *MPXV5004* pressure sensor from Freescale Semiconductor, Inc., with a measuring range of 0 kPa to 3.92 kPa, is selected since it has the characteristics mentioned above, its measuring range is in accordance with the expected IPRA differential pressure interval and is appropriate for MCU based systems.

4.1.3.1 Calibration

The *MPXV5004* output voltage is acquired by the *Arduino Uno* 10-bit Analog-to-Digital Converter (ADC). Its voltage input range is 0 V to 5 V and the resolution is 4.88 mV. The 5 V correspond to the maximum range of the pressure sensor, 3.92 kPa and, considering the *Arduino Uno* resolution, the minimum differential pressure value the pressure control system is able to detect is 3.83 Pa. The sensor *MPXV5004* was calibrated using a water column. The output voltage of this sensor was sampled for water column heights from 0 cm to 24 cm. The relationship between a water column height, h, and pressure, P, is described in equation 4.1. Using this equation, the output voltage data points of the sensor are matched to a certain pressure, blue line of figure 4.3. The transfer

function of the sensor *MPXV5004*, figure 4.3, is obtained by drawing a tendency line over these points, which were shifted to start at (0,0), and it is identified in equation 4.2.

$$P = g \cdot \rho \cdot h \tag{4.1}$$

g = gravitational acceleration
ρ = density

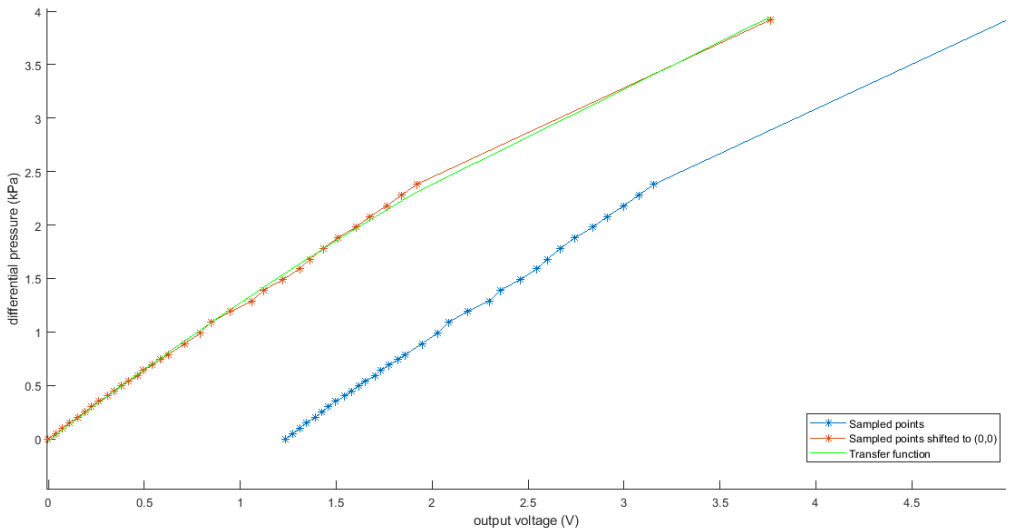

Figure 4.3: Differential pressure sensor transfer function

$$P = -0.0219 \cdot (V - 1.236)^3 + 0.0272 \cdot (V - 1.236)^2 + 1.2503 \cdot (V - 1.236) \tag{4.2}$$

P = differential pressure
V = voltage

4.1.4 Electronic valve

Valves are used to regulate a fluid flow, in this case air flow. Solenoid valves, an electronic valve type, are controlled by electrical signals. A normally close solenoid valve is closed, no fluid can flow through the valve, in its normal state and is open, fluid can flow through the valve, when an electrical signal is applied to it. Opposite logic applies to a normally open solenoid valve. Commercially, there is a wide range of solenoid valves available operating at 12 V, 24 V and at other supply voltages. A normally close solenoid valve, operating at 12 V, is chosen since the objective is to not let any air leak from the IPRA. In this way, power consumption only occurs if there is a need to lower the IPRA pressure. A relief valve, a safety valve type, is a mechanical valve designed to protect systems from over pressure. This valve is normally close, and opens when the pressure is above a certain threshold. A relief valve is incorporated in the pressure control system

since it is a safe way of ensuring the IPRA does not burst in case the electronic valve does not work.

4.2 Software

Figure 4.4 contains a block diagram describing the different logic connections between the several entities that compose the pressure control system, responsible for controlling the pressure inside the IPRA. The MCU is connected to a computer using a serial interface, establishing a communication link. Two software programs were implemented. One is responsible for the IPRA pressure control, run on the MCU, and, the other one, is responsible for monitoring the data collected by the MCU and for transmitting commands to the MCU. The programming language C++ was used in the software program developed for the computer. The software present on the MCU was implemented in C, using the microcontroller integrated development environment *Arduino IDE* and *Arduino* libraries when appropriate.

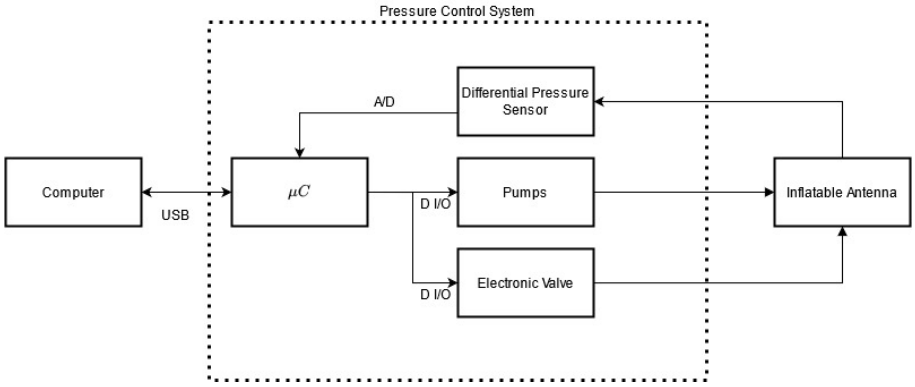

Figure 4.4: Inflation monitoring logic block diagram

The pressure control system software contains two operation modes: manual and automatic (default mode). To alternate between the modes, a serial command is transmitted to the MCU from a computer. The manual mode allows to have full control of the IPRA inflation: the user can decide when to turn *on* or *off* the air pumps or the electronic valve. The automatic mode, as the name suggests, automatically controls the IPRA inflation. The IPRA pressure is monitored by the differential pressure sensor which output data is acquired by the MCU ADC. Based on the measured pressure, the automatic mode actuates on the pumps and electronic valve in order to maintain the IPRA pressure inside the optimal differential pressure interval. This interval, [*Threshold 1*, *Threshold 2*]Pa, is derived from the results obtained from simulations previously conducted (section 3.2.4) . The pumps are actuated when the IPRA is considered under inflated: its pressure is lower than *Threshold 1*. When the IPRA pressure is higher than *Threshold 2* the pumps are set to the *off* state. This ensures the pressure is kept between the optimal differential pressure interval. The electronic valve and the air pumps are never actuated at the same time. In fact, the electronic valve is actuated considering another pressure value, *Threshold 3*, higher than *Threshold 2*. If the IPRA is over inflated, its pressure is higher than *Threshold 3*, the electronic

valve is actuated, otherwise it is in the *off* state. The pumps and the electronic valve act according to a enable/disable state, during which the components can only be active during the enable state. The change between these two states is controlled by commands sent by the user. This ensures complete control over the pressure control system and prevents unwanted changes to the state of the actuators. Furthermore, the user has an option to modify the differential pressure thresholds by transmitting a serial command.

In order to exchange data between the MCU and the computer a simple communication protocol was implemented. There are two distinct type of packets, defined by their content: data packets and command packets. Data packets contain information about the pressure control system and are transmitted from the MCU to the computer. Command packets contain commands to alter the state of the pressure control system and are transmitted from the computer to the MCU. Figure 4.5 shows the structure of these packets.

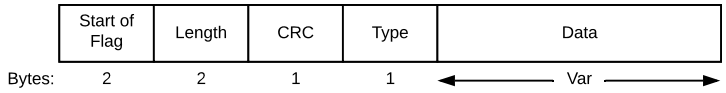

Figure 4.5: Structure of transmission packets

Every packet "Start of Flag" is defined as `0xAA 0x77`, while the "Length" field contains the size of the "Data" field, using a little-endian representation. A Cyclic Redundancy Check (CRC) is used to detect possible transmission errors. The "Type" field will be used to specify the type of information being transmitted, table 4.1.

Table 4.1: Type entities identifiers

Packet Content - Data	**Type**
Electronic Valve	`0x08`
Pump 1	`0x09`
Pump 2	`0x0E`
Differential pressure - Current reading	`0x0B`
Differential pressure - Threshold 1	`0x0C`
Differential pressure - Threshold 2	`0x0D`
Differential pressure - Threshold 3	`0x04`
Packet Content - Command	**Type**
Electronic Valve	`0x18`
Pump 1	`0x19`
Pump 2	`0x1E`
Differential pressure - Threshold 1	`0x1C`
Differential pressure - Threshold 2	`0x1D`
Differential pressure - Threshold 3	`0x14`

On the command packets, the "Data" field structure contains different values depending on the command to be transmitted to the MCU. To enable/disable or turn on/off the electronic valve

and pumps entities the following encoding is used, table 4.2. The possibility to turn *on* or *off* the automatic pressure control system is defined as well.

Table 4.2: Command values, "Data" field

Command	**Value**
Enable	`0x21`
Disable	`0x20`
On	`0x11`
Off	`0x10`
Automatic Off	`0x31`
Automatic On	`0x30`

The following figures summarize the possible transmitted packets. Figure 4.6 represents a command packet with the purpose to change the state of the pumps, electronic valve or of the automatic pressure control.

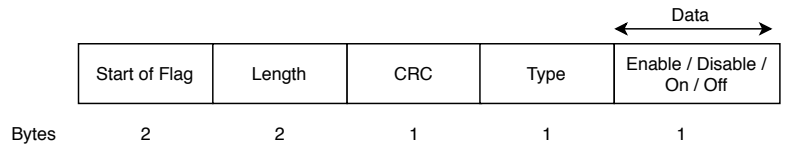

Figure 4.6: Structure of command packets for pumps, electronic valve or automatic pressure control state

Also, to transmit the state of these entities from the MCU to the computer, the data packet is described in figure 4.7.

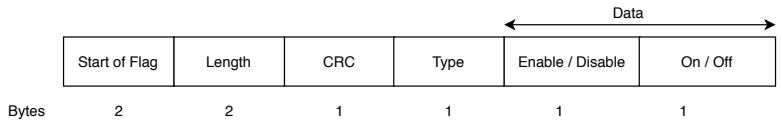

Figure 4.7: Structure of data packets for pumps and electronic valve

To transmit the current value of the differential pressure sensor reading, in kPa, or change the pressure control thresholds a packet with the structure of figure 4.8 is used.

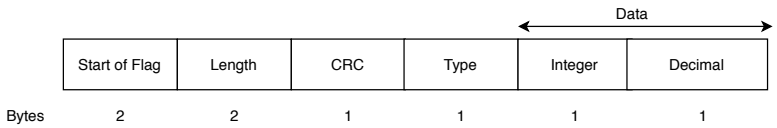

Figure 4.8: Structure of command/data packets relative to pressure values in kPa

Chapter 5

Tests and Results

This chapter describes all performed tests and consists of three subsections. The first one describes the tests performed to the pressure control system. The second one includes the tests carried out to evaluate the manufactured IPRA inflation. The last subsection describes the RF characterization of the manufactured IPRA.

5.1 Pressure control system

Throughout a stratospheric flight the pressure control system will experience a variation of ambient pressure, from MSL to around 1000 Pa, corresponding to an altitude of 31 km. The pressure control system must be capable of operating in this pressure range to ensure proper antenna inflation. A test was performed in the vacuum chamber of the Department of Chemical Engineering of the Faculty of Engineering of the University of Porto. It consisted in remotely controlling the air pumps and electronic valve inside the vacuum chamber in order to pump or remove air from a container at different ambient pressures. By monitoring the differential pressure, $P1 - P0$, between the container, $P1$, and the pressure inside the vacuum chamber, $P0$, one can indirectly calculate a pump volumetric flow rate and leakage rate of the pressure control system with its components disabled, figures 5.1a and 5.1b, respectively. The tests scenarios, figure 5.1, were repeated for 5 different values of ambient pressure: 1 kPa, 2 kPa, 10 kPa, 20 kPa and MSL. After determining a pump volumetric flow rate at distinct ambient pressures, one can calculate the time needed to inflate the antenna at each condition.

(a) Determination of a pump volumetric flow rate (b) Determination of the system air leakage

Figure 5.1: Vacuum chamber testing scenarios

According to the ideal gas equation, the amount of substance is equal to:

$$n = \frac{P \cdot V}{R \cdot T} \tag{5.1}$$

$P =$ absolute pressure
$V =$ volume
$R =$ universal gas constant
$T =$ temperature

For a constant volume and temperature, $\dot{n}$ is:

$$\dot{n} = \dot{P} \cdot \frac{V}{R \cdot T} \tag{5.2}$$

Assuming the amount of substance, which goes through a pump is the same, figure 5.1a, a pump volumetric flow rate can be obtained using the equation 5.3. With the vacuum chamber, one can control the value of the ambient pressure, P_0. The differential pressure of the container was set to increase from 0 Pa to 3.92 kPa. The value 3.92 kPa was chosen since it is the differential pressure sensor full scale value. Due to size limitations of the vacuum chamber, the container is made of four hard-plastic bottles of 0.5 L, corresponding to a total of 2 L.

$$\dot{V_0} = \dot{P_1} \cdot \frac{V_1}{P_0} \tag{5.3}$$

$\dot{V_0} =$ volumetric flow rate
$P_0 =$ ambient pressure
$P_1 =$ container pressure
$V_1 =$ container volume

To estimate the system with the air pumps and electronic valve disabled, leakage rate, figure 5.1b, one can also use the equation above, 5.3. Here, $\dot{V_0}$ corresponds to leakage rate.

The results from the vacuum chamber test, presented in the following two subsections, demonstrate the pressure control system can operate at the desired ambient pressure range. Figure 5.2 shows the test set up and only one pump was used to increase the pressure of the container.

Figure 5.2: Vacuum chamber test pressure control system set up

5.1.1 Pump characterization

As the ambient pressure, $P0$, decreases, the container pressure takes longer to reach the target differential pressure of 3.92 kPa, figure 5.3. Nevertheless, each pump was capable to provide the required pressure at the different ambient pressures. From figure 5.3 it can be observed the differential pressure of the container follows an exponential trend, described by equation 5.4, and there exists a maximum differential pressure which a pump can provide at different ambient pressures. Using the *Matlab* function *fit()*, with the equation 5.4 as its fitting function , the exponential curves were estimated, in dashed black lines (figure 5.3), and the values of ΔP_{max} and τ extracted, table 5.1.

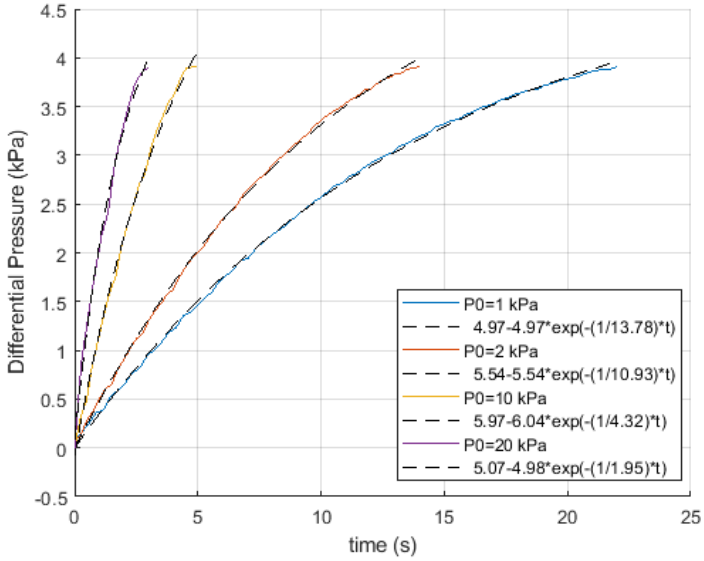

Figure 5.3: Differential pressure of the container vs time at different ambient pressures

$$\Delta P = \Delta P_{max} - K \cdot e^{\frac{-t}{\tau}} \tag{5.4}$$

Table 5.1: Estimated values of ΔP_{max} and τ for different ambient pressures

P_0(kPa)	ΔP_{max} (kPa)	τ (s)
1	4.97	13.78
2	5.54	10.93
10	5.97	4.32
20	5.07	1.95

The equation 5.3 can be rewritten as a function of $\dot{\Delta P}$:

$$\dot{V_0} = \dot{\Delta P} \cdot \frac{V_1}{P_0} \tag{5.5}$$

Furthermore, one also knows:

$$\tau \cdot \dot{\Delta P} + \Delta P = \Delta P_{max} \tag{5.6}$$

Replacing $\dot{\Delta P}$ in equation 5.5, the volumetric flow rate of a pump can be expressed as a function of ambient pressure, P_0, and of ΔP.

$$\dot{V_0}(P_0, \Delta P) = \frac{V_1 \cdot \Delta P_{max}}{P_0 \cdot \tau} \cdot (1 - \frac{\Delta P}{\Delta P_{max}}) \tag{5.7}$$

Figure 5.4 shows the calculated pump volumetric flow rate for different ambient pressures, with V_1 equal to the container volume (2 L).

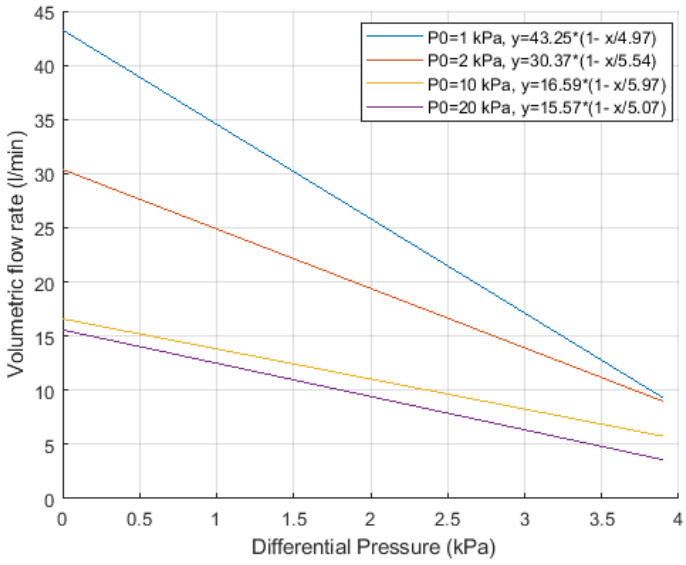

Figure 5.4: Pump volumetric flow rate at different ambient pressures

Analysing the pump volumetric flow rate, it is possible to conclude its performance decreases with the increase of the entity pressure it is pumping air into. This is more emphasized in low ambient pressures. The estimated times to inflate the IPRA, circa 300 L, using one pump of the

pressure control system are identified in table 5.2 for $\Delta P = 0$ Pa and $\Delta P = 1$ kPa. 0 kPa to 1 kPa is the expected operating pressure range of the pressure control system. The volumetric flow rates, at ambient pressures lower than MSL, demonstrate the pressure control system pumps are capable of inflating the IPRA under the 40 min requirement mentioned in section 4.1.2. Even though, these times correspond to the duration of pumping 300 L of air, with ΔP equal to 0 Pa and 1 kPa, they provide an approximate lower and maximum duration one can expect it will take to inflate the antenna. Furthermore, one must also consider the friction forces the air experiences in the components it goes through which connect the pump outlet to the IPRA. These friction forces originate pressure loss [37], dependent of the fluid flow regime, which needs to be accounted. The higher a pipe length is, the higher the pressure loss will be. The presence of a pressure drop means the pump needs to provide more air to the IPRA to reach the same ΔP if no pressure drop was present in the system. There can be the case where the pump is not capable of overcoming the losses and the IPRA pressure will not increase. Therefore, due to the presence of pressure drops, the approximated maximum duration to inflate the antenna is increased by a factor of Δt, dependent on the system pressure drop.

P_0 (kPa)	**Altitude** (km)	**Inflation time** (min), $\Delta P = 0$ Pa	**Inflation time** (min), $\Delta P = 1$ kPa
1	31	7	9
2	26	10	12
10	15	18	22
20	10	20	24
MSL	0	57 (from manufacturer)	57 (from manufacturer)

Table 5.2: Estimated antenna inflation for different ambient pressures, using one pump of the pressure control system

5.1.2 System air leakage rate

Initially, the differential pressure inside the container was set to 3.92 kPa. $P1$ will start to decrease in the presence of leakages in the system (pumps, valve, differential pressure sensor and bottles). The system differential pressure through time is shown in figure 5.5 for different ambient pressures. A linear tendency line was determined based on the recorded data at each ambient pressure. The line slope corresponds to $\dot{P}_1$ with its values identified in figure 5.6a, and the leakage rate is determined using equation 5.3. Moreover, as expected, with the decrease of ambient pressure, $\dot{P}_1$ is smaller, since number of particles that exit the container is lower. At the several ambient pressures, 1 kPa, 2 kPa, 10 kPa, 20 kPa and MSL, the leakage rate is small, around 10^{-4} L/min. No major leakages, with origin in one of the pumps, electronic valve or differential pressure sensor, were detected. The leakage main source is assume to be the bottle cap, where the air tubes are connected. One can conclude when the air pumps and electronic valve are disabled, they do not act as active leakage sources.

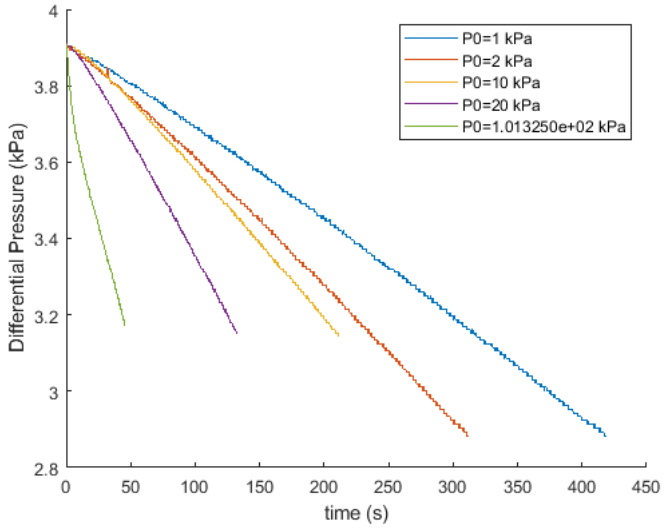

Figure 5.5: Differential pressure of the container vs time at different ambient pressures, with both pumps off

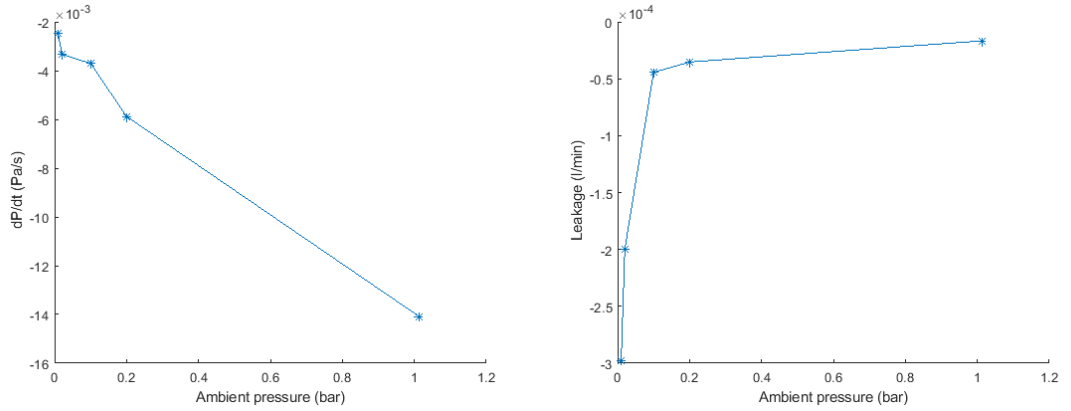

(a) $\dot{P}_1$ at different ambient pressures (b) System leakage at different ambient pressures

Figure 5.6: System leakage characterization

5.1.3 Differential pressure control

During the vacuum chamber test where the ambient pressure was 2 kPa the automatic mode of the pressure control system was tested, figure 5.7. The differential pressure interval was set to be between 1.25 kPa (*Threshold 1*) and 2 kPa (*Threshold 2*). At the end of the test, the electronic valve was manually actuated, via command, to verify its correct functionality.

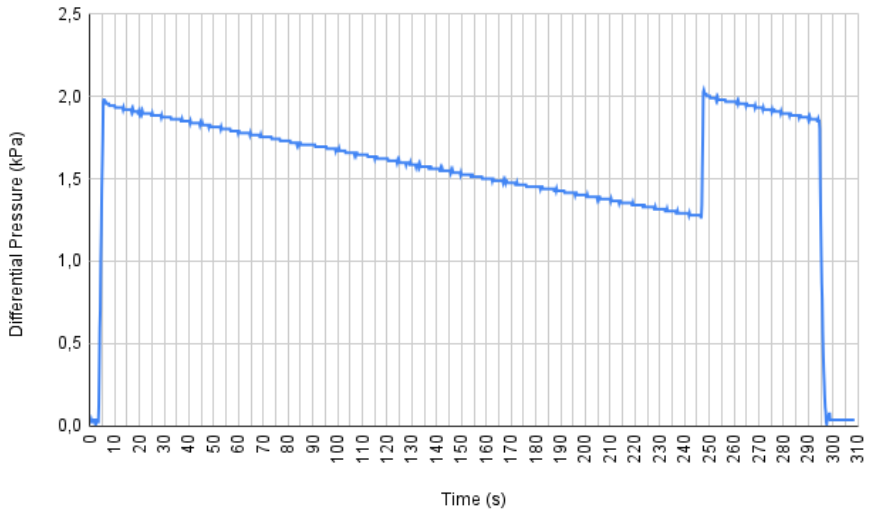

Figure 5.7: Differential pressure control

With a larger container, one would better observe the differential pressure increase since it would be even slower. Nevertheless, the pressure control system is capable of maintaining the differential pressure of the container inside the desired interval. When controlling the pressure of the IPRA, its differential pressure increase is slower, thus, the sensor will be able to better monitor this change. Resulting in a finer control with a tighter interval.

5.2 Antenna inflation

The first test consisted in inflating the manufactured antenna, without using the air pumps from the pressure control system, in order to assess the inflated shape of the manufactured IPRA, an air compressor was used instead, figure 5.8. No major leakage was detected which prevented the antenna inflation.

(a) Reflector view, antenna over inflated (b) Desired shape

Figure 5.8: Inflatable antenna shape when inflated using an air compressor

The manufactured antenna inflated into a shape similar to the one simulated in section 3.2.4, figure 5.9. In the IPRA reflector centre, the Mylar® is smooth without many wrinkles. In addition, the reflector periphery concentrates the majority of wrinkles, specially at the seams. Even though they are more pronounced in the real antenna, *Abaqus/FEA* was able to identify the potential locations where the antenna would suffer more deformations.

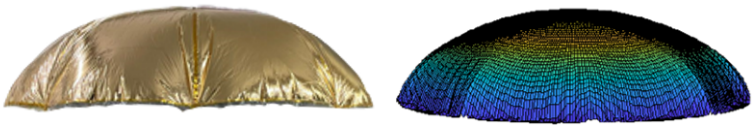

Figure 5.9: Comparison between real reflector (left) and *Abaqus/FEA* simulated reflector shape (right)

The pressure of the antenna was monitored using the differential pressure sensor, figure 5.10. Through visual inspection, at a differential pressure from 40 Pa to 100 Pa, the antenna was already well inflated, with some margin to increase the pressure. However, above 250 Pa, the antenna started to become too stretched, figure 5.8a, and at 325 Pa the Kapton® tape no longer could hold the antenna in place. The Kapton® tape started to detach from some Mylar® and plastic juxtapositions. The *Threshold 3* value, above which the electronic valve is turned on, was set at 300 Pa. Wrinkles are present at the junctions between Mylar® and plastic. These "V" wrinkles between each bud are assumed to be a consequence of the manufacturing method. It is believed if the buds are cut using the same wooden molds but with some added lateral margin, the buds will experience less stress once placed on the curvature molds, minimizing the "V" wrinkles at these regions.

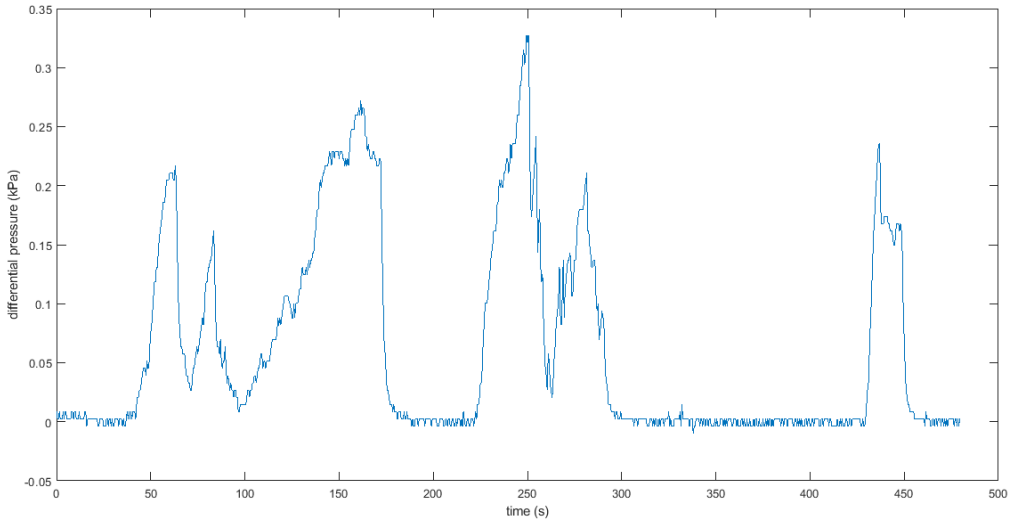

Figure 5.10: IPRA differential pressure measured, using an air compressor to inflate the antenna

The following inflation test replaced the air compressor with the air pumps, manually controlled, with the goal of determining if these air pumps are capable of inflating the IPRA to the same differential pressures registered with the air compressor. In around 30 min, the air pumps were capable of inflating the antenna to the desired shape. However due to the presence of air leakages on the IPRA, the obtained shape had less air volume, figure 5.11, than the one achieved with the air compressor. Furthermore, the maximum differential pressure recorded was 30 Pa. With this result, the automatic pressure control was prevented from bringing the antenna pressure to the desired differential pressure interval estimated in section 3.2.4. The IPRA back support demonstrated to be effective when the IPRA was tilted 45°. The greater the volume of the IPRA, the better this support held the antenna in place, not allowing it to move to its sides.

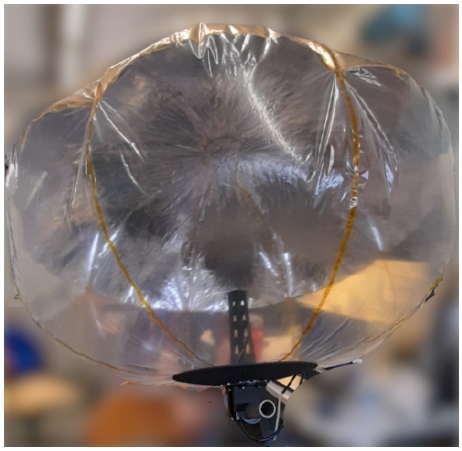

Figure 5.11: Inflatable antenna shape when using air pumps to inflate it

5.3 Inflatable antenna characterization

The IPRA was characterized on the anechoic chamber of the Faculty of Engineering of the University of Porto. A Vector Network Analyzer (VNA) with two ports, *Port1* and *Port2*, was used to sweep a frequency between 4.8 GHz and 6.8 GHz, with the frequency of interest at 5.8 GHz. A vivaldi antenna, figure 5.12, with vertical polarization was used as the transmit antenna (Tx), connected to *Port1*.

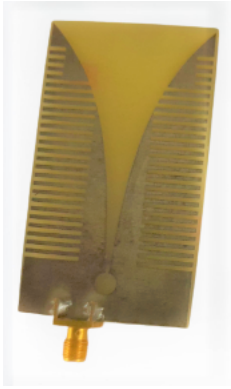

Figure 5.12: Vivaldi antenna

The receive antenna (Rx) is connected to *Port2* and acts as the Antenna Under Test (AUT). The power, in dBm, received at Rx, can be calculated using the Friis equation, 5.8.

$$P_{Rx_{dB}} = P_{Tx} + G_{Tx} + G_{Rx} + FSL \tag{5.8}$$

If one knows the distance, d, between the two antennas, the Free Space Losses, FSL, can be calculated using the following equation:

$$FSL_{dB} = 20\log_{10}(\frac{\lambda}{4 \cdot \pi \cdot d}) \tag{5.9}$$

The S-parameter, $S_{21} = P_{Rx} - P_{Tx}$, measured by the VNA corresponds to:

$$S_{21_{dB}} = G_{Tx} + G_{Rx} + FSL \tag{5.10}$$

Using another vivaldi antenna as an AUT, one can obtain the gain of each, since:

$$G_{Vivaldi_{dB}} = \frac{S_{21} - FSL}{2} \tag{5.11}$$

The distance between the two vivaldi antennas was 4.3 m , $FSL = -60.4dB$ at 5.8 GHz, and the measured S_{21} was -44.8 dB. Using equation 5.11, the gain of one vivaldi antenna is approximately 8 dBi at 5.8 GHz, figure 5.13.

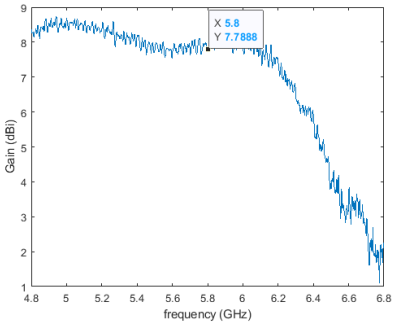

Figure 5.13: Vivaldi antenna gain

With this, the gain of an AUT can be determined using equation 5.12:

$$G_{AUTdB} = S_{21} - G_{Vivaldi} - FSL \tag{5.12}$$

5.3.1 Inflatable antenna as AUT

The antenna was mounted in the anechoic chamber perpendicular to the ground, figure 5.14. The antenna support was not designed to hold the antenna in this way. A small tape was placed in the bottom part of the antenna and taped to the anechoic chamber wooden support, as seen in figure 5.14c, preventing the antenna from leaning back. The maximum possible distance between the IPRA and the vivaldi antenna is 5.2 m. At these distances, the IPRA is still in its near field region.

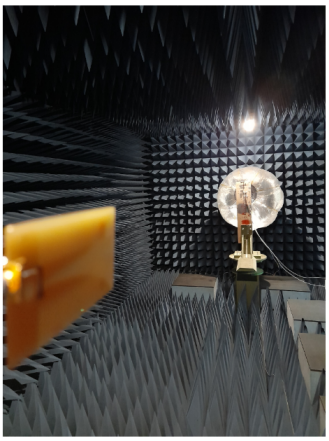

(a) Inflatable antenna as AUT

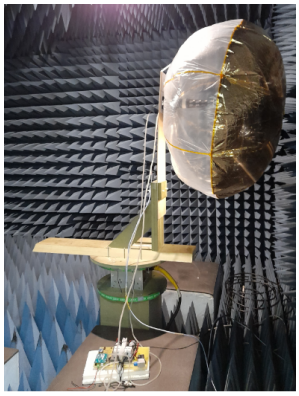

(b) Inflatable antenna installed inside the anechoic chamber

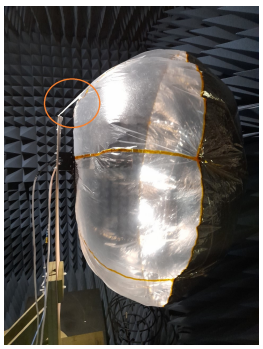

(c) Inflatable antenna taped to the wooden support, highlighted in orange

Figure 5.14: Inflatable antenna installed inside the anechoic chamber

With the multiple inflation and deflation cycles the antenna was subject to, prior its RF characterization, the antenna integrity was affected and the air leakages started to be relevant. The air pumps were no longer able to inflate the antenna as previously. To overcome this, an additional small air blower was used to continuously pump air into the IPRA. The feed height used was 24 cm and the antennas were distanced 4.9 m, $FSL = -61.51dB$ at 5.8 GHz. The IPRA radiation pattern

is shown in figure 5.15 with the main lobe well defined. The peak gain in the horizontal polarization is 23.48 dBi and in the vertical polarization is 23.77 dBi. In addition, the IPRA beamwidth at -3 dB is 6°.

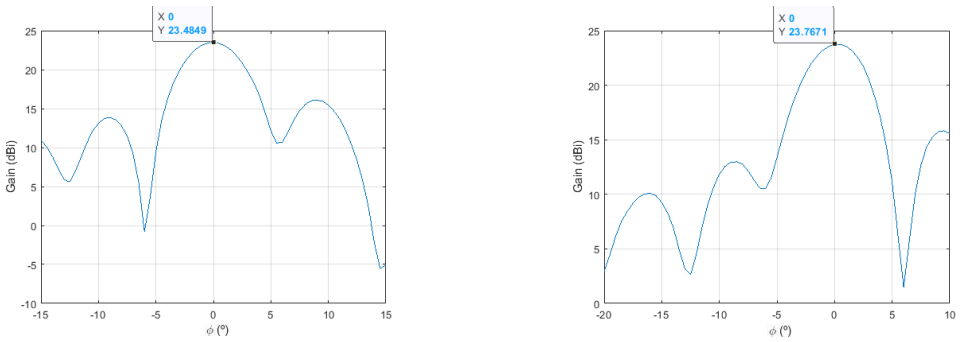

(a) Horizontal polarization (b) Vertical polarization

Figure 5.15: IPRA radiation pattern at 5.8 GHz

The above results were obtained with the antenna not filled to its maximum pressure, identified in section 5.2. The differential pressure recorded by the sensor was variable between 20 Pa and 40 Pa. The maximum measured gain of 23.77 dBi is lower than the maximum simulated gain, 29.38 dBi. The difference is around 5.6 dBi. It should be noted the antenna will have a different behaviour when it is tilted at 45° NADIR, however in the anechoic chamber it was not possible to mount it in this way. It was, instead, tilted at 90°, this is one of the main reasons why the IPRA full performance was not obtained. The manufacturing errors, such as bud misalignment and bud manual cutting, originate changes to the IPRA shape and have an important contribution to gain loss. Nevertheless, the possibility of the used patch antenna not being the most well adapted feed for this type of antenna is also considered. Furthermore, the IPRA was not completely perpendicular to the ground, even though a tape was used to minimize this effect. The IPRA was slightly leaned back which resulted in its reflector not facing the Tx antenna from the front. This affects the IPRA radiation pattern, shifting the main lobe away from the intended direction. In this situation, instead the IPRA being directly pointed to the Tx antenna, it must be deviated in some degree. Another observation, besides the antenna being leaned back, is the IPRA was below the optimal position. In this situation, the feed has a positive vertical shift relative to its original position. Figure 5.16a looks to represent this: in green is highlighted the original feed position and in blue the positive feed shift relative to the antenna displacement. A simulation was performed on the IPRA model, from section 3.2, to determine the influence of the IPRA reflector not being completely aligned with its feed, figure 5.16b. As one can see, for the original feed position (*feed offset* $= 0$ m), the more the IPRA is leaned back, the higher the gain loss is. The fact that, at the same time, the IPRA is below the original feed position (*feed offset* >0 m) is beneficial since it minimizes this gain loss as well as contradicts the main lobe shift. During the IPRA RF characterization the antenna was tilted approximately 10° to 15°, this indicates an estimated gain loss of 0.5 dB to 0.8 dBi.

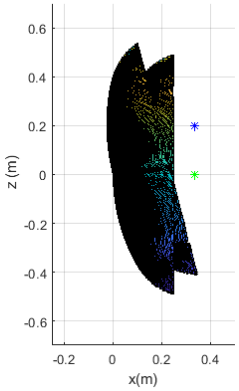

(a) Influence of the IPRA inclination on the feed position

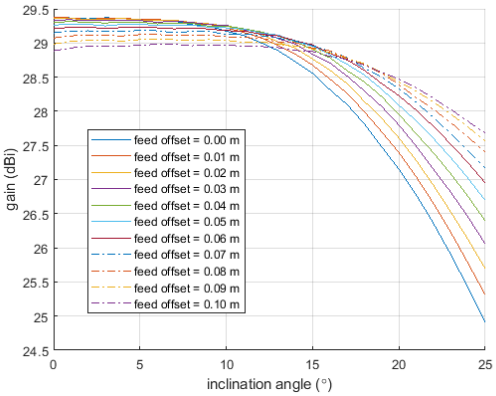

(b) Inclination angle vs RF performance

Figure 5.16: Influence of the IPRA inclination in its RF performance

5.3.2 Dish antenna as AUT

A dish antenna with a diameter of 0.7 m was also characterized at the anechoic chamber, figure 5.17.

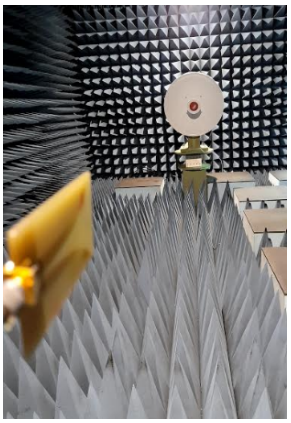

Figure 5.17: Dish antenna as AUT

The tested antenna is a mANT30 from MikroTik with a typical gain of 30 dBi for a frequency range of 4.7 GHz to 5.8 GHz. The vivaldi antenna and this AUT were 4.15 m apart. The measured radiation patterns for the vertical and horizontal polarization are shown in figure 5.18.

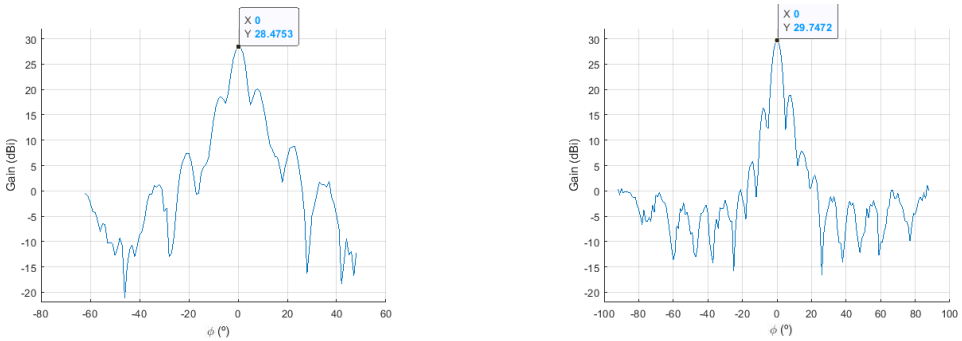

(a) Horizontal polarization (b) Vertical polarization

Figure 5.18: Dish antenna radiation pattern at 5.8 GHz

This antenna has a better performance when the vertical polarization is used, with the antenna gain, 29.7 dBi, close to the one mentioned by the manufacturer. Furthermore, its beamwidth at -3 dB is 5°.

5.3.3 Comparison between the IPRA and dish antenna

The radiation pattern of the IPRA is compared with the one from the dish antenna in figures 5.19 and 5.20 for the horizontal and vertical polarization, respectively.

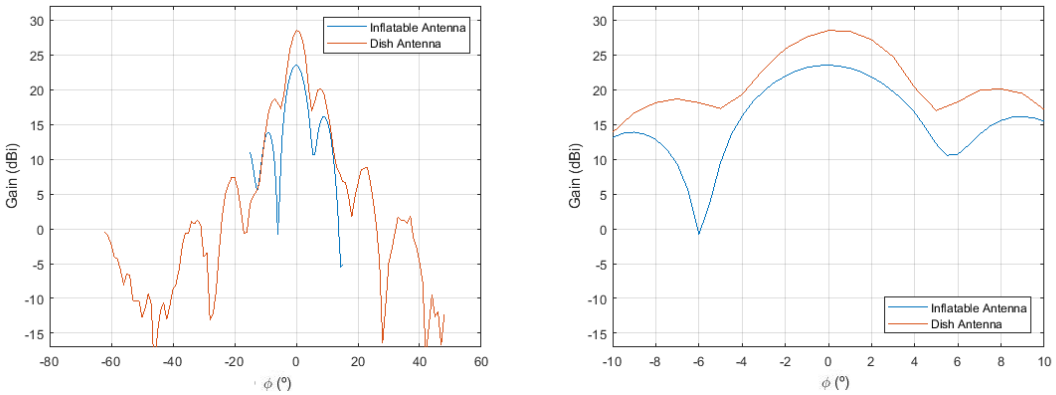

(a) Radiation pattern (b) Main lobe

Figure 5.19: Comparison between IPRA and dish antenna at 5.8 GHz: horizontal polarization

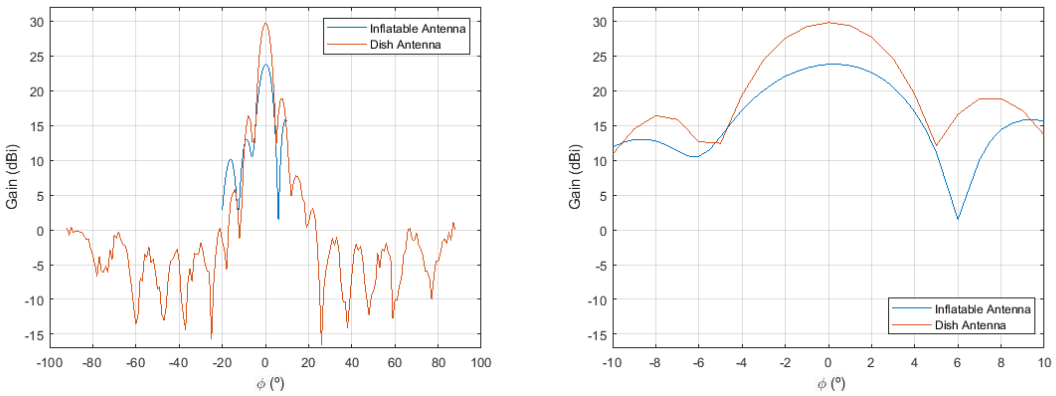

(a) Radiation pattern

(b) Main lobe

Figure 5.20: Comparison between IPRA and dish antenna at 5.8 GHz: vertical polarization

Clearly, the IPRA radiation pattern resembles the pattern of a fixed reflector, with a main lobe well defined. Nevertheless, its wider beamwidth, 6°, indicates that not all reflective area of the IPRA is being used. Moreover, the IPRA, gain of 23.77 dBi, is less efficient than its counterpart, gain of 29.7 dBi.

Chapter 6

Final remarks

6.1 Difficulties encountered

During the development of this thesis there were some difficulties. Initially, there was a challenge in how to import a *Matlab* generated surface to *Abaqus/FEA* , without deforming it. This challenge was overcome by generating a surface with extra margins which later are removed in *Abaqus/FEA* . Another challenge was the fabrication of the wooden molds as there was no appropriate machinery available to cut it precisely, an external company was contacted and offered its services. Moreover, the lack of a 3d printing machine available for students prevented the experimentation of different antenna and feed support configurations. Due to the presence of leakages in the inflatable antenna, the chosen air pumps could not provide enough air to allow the control of the antenna pressure as well as to measure its RF properties at different pressures. Moreover, with the antenna being subject to multiple inflation and deflation cycles, the amount of leakages started to be considerable and the chosen air pumps were no longer able to inflate the antenna with enough air to obtain a defined shape. Finally, the characterization of the inflatable antenna in its far field region was not possible since one needed software defined radio capable of operating at 5.8 GHz did not exist at the faculty.

6.2 Conclusions

Inflatable reflector antennas are competitive with fixed reflector antennas in terms of weight, price and storage ratio. The study presented in this document describes the design and implementation of an inflatable reflector antenna at 5.8 GHz with a diameter of 1 m. This antenna is intended to be incorporated in the student project SARIA, acting as one of the antennas used to create SAR images throughout a stratospheric flight of the BEXUS gondola in the context of the REXUS/BEXUS programme cycle 13.

The design of the antenna as well as its simulation model are presented. FEM was used to simulate the IPRA characteristics. The FEA software *Abaqus/FEA* was selected to simulate the shape of the IPRA, at several differential pressures. A *Matlab* script was used to compute the

IPRA reflector radiation pattern. With these tools, one was capable of estimating with success the IPRA shape, gain and differential pressure interval which allows to take full advantage of its RF performance at 5.8 GHz. The manufacturing of the inflatable antenna was done by hand using wooden molds for assistance and COTS materials were used.

The IPRA pressure control system is presented with the selection of hardware taking into account it must be suitable for low pressure environments. Regarding software, two controlling modes were implemented allowing the user to choose between automatic and manual inflation. Tests were conducted on a vacuum chamber to characterize the air pump volumetric flow rate and system leakage. Results show the selected hardware is capable of operating in low ambient pressures.

The IPRA inflation was achieved using two different methods: an air compressor and the pressure control system. With the air compressor, one was able to identify the physical limits of the manufactured antenna and the possible working differential pressure values. However, with the pressure control system, one could not observe the previous scenario as the presence of air leakages prevented the antenna inflation to differential pressures above 30 Pa. Inflation test results show *Abaqus/FEA* was capable of correctly simulating the inflatable antenna shape.

In order to characterize the manufactured inflatable antenna, the anechoic chamber available in faculty was used. The anechoic chamber did not have the conditions to mount the antenna at 45° NADIR, which prevented the characterization of its full performance. The antenna was, instead, mounted at 90°. The maximum measured gain, 23.77 dBi, is about 5.6 dBi lower than the simulated one, reason why it was presented an explanation for this gain loss.

The IPRA was subjected to several manipulation cycles, and its extensive use has led to possible deformations in its physical structure, originating more air leakage sources. From the point of view of controlling the pressure of the IPRA using the pressure control system, the results were not desired since due to air leakage the antenna differential pressure did not go above 30 Pa. This implies the manufactured IPRA and future IPRAs should be managed with precaution and over inflating the antenna should be avoided.

This study main objective was partially achieved since it was not possible to fully control the IPRA differential pressure. More tests are necessary to completely validate the system. Nevertheless, this works contributes to the expertise of developing inflatable antennas for low pressure ambient applications and in orbital environment applications.

6.3 Future work

Interest for inflatable antennas is growing because they are capable of operating as fixed antennas with lesser cost and weight. The work developed here looks to contribute to a fully operational inflatable antenna model at 5.8 GHz.

The leakage of the manufactured IPRA was a problem throughout the final phases of this work. Optimizing the manufacturing method will contribute to minimize them as well as improve the final inflated shape. An inflatable antenna with less leakage will allow the current pressure control

system to control the IPRA pressure, enabling the characterization of the antenna RF properties at several differential pressure values.

The proposed IPRA simulation model can be explored in different fronts. One can look to optimize the number of buds which form the reflector and the canopy of the IPRA. Increasing the number of buds will make these structures tend more towards the desired design curves. Another area worth exploring is the optimization of the material thickness, thinner materials will produce a lighter antenna, although it may be more fragile. The simulation model can be improved by reverse engineering the manufactured IPRA to obtain its initial non inflated configuration.

Further tests are still necessary to fully characterize the inflatable antenna. Characterization of the inflatable antenna in its far field, with the possibility of controlling its differential pressure, will better assess the performance of the proposed IPRA model. Possibly, using near field measuring techniques which results can be transformed to the far field. The antenna characterization should take into account the IPRA is to be mounted 45° NADIR. Environment testing such as inflating the antenna in a vacuum chamber will inform how the IPRA behaves at low ambient pressures similar to the ones experienced on a stratospheric flight. One can also study and optimize the storage of the proposed inflatable antenna model.

The SARIA experiment is set to participate on the stratospheric flight of the BEXUS 31 gondola in late September 2021. The use of this IPRA on such scenario will allow to assess its use as an antenna for SAR applications in low pressure environments.

Bibliography

[1] Gonçalo Santos. "SAR Algorithms for Embedded Platforms". Master's Thesis. Faculty of Engineering of the University of Porto, 2021.

[2] Tiago Martins. "RF Front-End for RADAR". Master's Thesis. Faculty of Engineering of the University of Porto, 2021.

[3] Yan Xu and Fu Ling Guan. "Structure design and mechanical measurement of inflatable antenna". In: *Acta Astronautica* 76 (July 2012), pp. 13–25.

[4] Hong Jian Wang, Fan Bin, Yi Min, Fu Ling Guan, Guang Liu, Chen Xue, Yan Xu, Jianguo Huang, Cai Minghui, and Liu Shihua. "Inflatable antenna for space-borne microwave remote sensing". In: *IEEE Antennas and Propagation Magazine* (2012).

[5] Naomi Mathers. "Inflatable Antennas for Portable Direct Satellite Communication". Bachelor of Engineering. RMIT University, Feb. 2010.

[6] Naomi Mathers. "Using inflatable antennas for portable satellite-based personal communications systems". In: *Space Technologies for the Benefit of Human Society and Earth*. 2009.

[7] R. E. Freeland and G. Bilyeu. "In-step inflatable antenna experiment". In: *Acta Astronautica* (1993).

[8] G. J. Friese, G. D. Bilyeu, and M. Thomas. *Initial '80s Development of Inflated Antennas*. Tech. rep. NASA, 1983.

[9] Bryan W. Welch. "Derivation of surface shape for inflatable large aperture antennas". In: *Mathematical Methods in the Applied Sciences* (2019).

[10] *Project Echo*. URL: https://www.nasa.gov/centers/langley/about/project-echo.html (visited on Jan. 4, 2021).

[11] *Echo 2*. URL: https://nssdc.gsfc.nasa.gov/nmc/spacecraft/display.action?id=1964-004A (visited on Apr. 13, 2021).

[12] I Robert Freeland, Steven Bard, Gordon Veal, Costa Cassapakis, Thomas Campbell, and M C Bailey. *Inflatable antenna technology with preliminary shuttle experiment results and potential applications*. Tech. rep. 1996.

[13] R. E. Freeland and G. R. Veal. “Significance of the inflatable antenna experiment technology”. In: *Collection of Technical Papers - AIAA/ASME/ASCE/AHS/ASC Structures, Structural Dynamics and Materials Conference*. 1998.

[14] R.A. Hoferer and Y. Rahmat-Samii. “RF characterization of an inflatable parabolic torus reflector antenna for space-borne applications”. In: *IEEE Transactions on Antennas and Propagation* 46.10 (1998), pp. 1449–1457. DOI: 10.1109/8.725276.

[15] Hui Feng Tan, Xiang Hong Bai, and Guo Chang Lin. “Surface accuracy measurement and analysis of an inflatable antenna by photogrammetry”. In: *Proceedings of 2011 Cross Strait Quad-Regional Radio Science and Wireless Technology Conference, CSQRWC 2011*. 2011.

[16] Alessandra Babuscia, Jonathan Sauder, Aman Chandra, and Jekan Thangavelautham. “ Inflatable Antenna for CubeSat ”. In: *CubeSat Antenna Design*. 2020. DOI: 10.1002/9781119692720.ch6.

[17] Alessandra Babuscia, Benjamin Corbin, Mary Knapp, Rebecca Jensen-Clem, Mark Van De Loo, and Sara Seager. “Inflatable antenna for cubesats: Motivation for development and antenna design”. In: *Acta Astronautica* (2013).

[18] Alessandra Babuscia, Thomas Choi, Jonathan Sauder, Aman Chandra, and Jekan Thangavelautham. “Inflatable antenna for CubeSats: Development of the X-band prototype”. In: *IEEE Aerospace Conference Proceedings*. 2016.

[19] Alessandra Babuscia, Jonathan Sauder, Aman Chandra, Jekan Thangavelautham, Lorenzo Feruglio, and Nicole Bienert. “Inflatable antenna for cubesat: A new spherical design for increased X-band gain”. In: *IEEE Aerospace Conference Proceedings*. 2017.

[20] Daniel S. Weile. “Handbook of reflector antennas and feed systems. volume 3: applications of reflectors [reviews and abstracts]”. In: *IEEE Antennas and Propagation Magazine* (2014).

[21] John Ruze. “Antenna Tolerance Theory—A Review”. In: *Proceedings of the IEEE* (1966).

[22] Bryan Welch. “Application of the Ruze equation for inflatable aperture antennas”. Master’s Thesis. Cleveland State University, May 2006.

[23] Jesse H. Mills, Alan J. Fenn, Sean Crowley, Bakari Hassan, Frank C. Robey, Pierre Dufilie, and Michael H. Hecht. “Space-Deployed Inflatable Dual-Reflector Antenna: Design and Prototype Measurements”. In: 33rd Annual AIAA/USU Conference on Small Satellites, 2019.

[24] Alan J. Fenn, Jesse H. Mills, Frank C. Robey, Pierre Dufilie, and Michael H. Hecht. “Axisymmetric Gregorian Reflector System for a Space-Deployed Inflatable Antenna: Simulations and Measurements”. In: *IEEE International Symposium on Phased Array Systems and Technology*. 2019.

[25] Jacob Fish and Ted Belytschko. *A First Course in Finite Elements*. 2007.

[26] Arthur L. Palisoc and Yuli Huang. “Design tool for inflatable space structures”. In: *Collection of Technical Papers - AIAA/ASME/ASCE/AHS/ASC Structures, Structural Dynamics and Materials Conference*. 1997.

[27] Aman Chandra, Jekanthan Thangavelautham, and Alessandra Babuscia. “Composite inflatable antennas for small - Satellites and backup communication”. In: *Ka and Broadband Communications Conference*. 2018.

[28] *Expeditionary SATCOM*. URL: https://www.cubic.com/solutions/c4isr/protected-communications/expeditionary-satcom%7B%5C%%7D5C%7B%5C#%7Dparagraph-tab-13-1 (visited on Dec. 27, 2020).

[29] *Inflatable Antennas Support Emergency Communication*. URL: https://spinoff.nasa.gov/Spinoff2010/ps%7B%5C_%7D5.html (visited on Dec. 27, 2020).

[30] Daniela Rus and Michael T. Tolley. *Design, fabrication and control of soft robots*. 2015.

[31] REXUS/BEXUS Programme. *Balloon EXperiments for University Students*. URL: http://rexusbexus.net/bexus/ (visited on June 28, 2021).

[32] M. Srinivasan, L. V. Kulkarni, and C. S. Pasupathy. “A simple technique of fabrication of paraboloidal concentrators”. In: *Solar Energy* (1979).

[33] Gary A. Stutzman Warren L. and Thiele. *Antenna Theory and Design, 3rd Edition*. 2013.

[34] *Abaqus Scripting Reference Guide (6.13)*. URL: http://130.149.89.49:2080/v6.13/books/ker/default.htm (visited on Apr. 7, 2021).

[35] Sven (2021). *stlwrite - write ASCII or Binary STL files*. URL: https://www.mathworks.com/matlabcentral/fileexchange/20922-stlwrite-write-ascii-or-binary-stl-files (visited on Apr. 5, 2021).

[36] Gonçalo Santos and Pedro Teixeira. *Antenas e Propagação - Antena patch de 5.8 GHz para feed de refletor parabólico insuflável*. 2020.

[37] Y. Cengel and Cimbala. *Fluid Mechanics: Fundamentals and Applications, 3rd ed*. 2010.